University of Dundee

MASTER OF SCIENCE

Mode-locked laser diodes for the 750 – 770 nm spectral region

Kong, Liang

Award date:
2015

UNIVERSITY OF DUNDEE

Mode-locked laser diodes for the 750 – 770 nm spectral region

Liang Kong

18/SEP/2015

Declaration

I, Liang Kong, hereby certify that this thesis, which is approximately 11688 words in length, has been written by me, that it is the record of work carried out by me and that it has not been submitted in any previous application for a higher degree.

Date 01/DEC/2015 Signature of candidate Liang KONG

I hereby certify that the candidate has fulfilled the conditions of the resolution and regulations appropriate for the degree of Master of Science by research in the University of Dundee and that the candidate is qualified to submit this thesis in application for that degree.

Date 01/DEC/2015 Signature of supervisor Maria Ana Catalina

Abstract

Ultrashort pulse lasers are widely used in research, industry, medicine, and communications, because of their characteristics of narrow pulse width, high repetition frequency, broad spectrum and high peak power. They are influencing and changing our world. Mode-locking is an effective way to generate ultrashort pulses. Semiconductor mode-locked lasers are excellent candidates for ultrashort pulse generation due to their advantages in compactness, weight, energy efficiency and cost. In this dissertation, we present the first demonstration of semiconductor mode-locked laser diodes in two wavebands – 750 nm and 760 nm. Both chips were based on an AlGaAs multi-quantum-well structure, with slight differences depending on the target spectral band.

At the 760 nm waveband, the laser diodes were passively mode-locked and generated pulses at around 766 nm, with pulse durations down to approximate 4 ps. They are designed with different laser cavity lengths of 1.815 mm and 1.515 mm, leading to the pulse repetition rates of 19.4 GHz or 23.2 GHz respectively.

Deep-red semiconductor monolithic mode-locked lasers are demonstrated, in the waveband of 750 nm. These lasers enable the generation of picosecond optical pulses at 752 nm, at pulse repetition rates of 19.37 GHz and 23.1 GHz, corresponding to 1.815 mm and 1.515 mm cavity lengths respectively. An investigation of the dependence of the pulse duration as a function of reverse bias revealed a predominantly exponential decay trend of the pulse duration, varying from 10.5 ps down to 3.4 ps. A 30-MHz-tunability of the pulse repetition rate with bias conditions is also achieved.

We checked the influence of the bias conditions on the mode-locking characteristics for these new lasers. It was also found that the front facet reflectivity played a quite important role in the possibility of mode-locking.

The demonstration of these compact, efficient and versatile ultrafast lasers in this spectral region paves the way for its deployment in a wide range of applications such

as bio-imaging, pulsed terahertz generation, microwave generation and millimeter-wave generation, with further impact on sensing, imaging and optical communications.

List of Publications

Journal publications

1. Huolei Wang, Liang Kong, A. Forrest, D. Bajek, S. E. Haggett, X. Wang, Bifeng Cui, Jiaoqing Pan, Ying Ding, and M. A. Cataluna, "Ultrashort pulse generation by semiconductor mode-locked lasers at 760 nm," *Optics Express*, vol. 22(21), pp. 25940-25946, 2014.

Selected for additional publication in the Virtual Journal for Biomedical Optics (VJBO) as Research Highlights, Vol. 9, Issue 12, Dec.2014

2. Liang Kong*, Huolei Wang* (both are the first authors), A. Forrest, D. Bajek, S. E. Haggett, X. Wang, Bifeng Cui, Jiaoqing Pan, Ying Ding, and M. A. Cataluna, "Deep-red semiconductor monolithic mode-locked lasers," *Applied Physics Letters*, vol. 105(23), 2014.

3. Mifeng Li, Haiqiao Ni, Ying Ding, David Bajek, Liang Kong, Maria Ana Cataluna, Zhichuan Niu, "Optimization of InAs/GaAs quantum-dot structures and application to 1.3-um mode-locked laser diodes," *Chinese Physics B* 23 (2), 027803 (2014).

4. Wang Huolei, Kong Liang, Pan Jiaoqing, Xu Tianhong, Ji Wei, Ni Haiqiao, Cui Bifeng, Ding Ying, "Recent Progress of Semiconductor Mode-Locked Lasers," *Laser & Optoelectronics Progress* 5, 050001-1-050001-14 (2013) (in Chinese)

Peer-reviewed conference proceedings

1. L. Kong, H. L. Wang, D. Bajek, S. Haggett, A. F. Forrest, X. L. Wang, B. F. Cui, J. Q. Pan, Y. Ding, M. A. Cataluna, "Semiconductor Monolithic Mode-locked Laser for Ultrashort Pulse Generation at 750nm". *24th IEEE International Semiconductor Laser Conference* (ISLC 2014).

2. H. L. Wang, L. Kong, D. Bajek, S. Haggett, X. L. Wang, B. F. Cui, J. Q. Pan, Y. Ding, M. A. Cataluna, "760-nm Semiconductor Passively Mode-Locked Monolithic Laser for Picosecond Pulse Generation". *CLEO: 2013*, San Jose, CA, USA (2013).

List of Figures

Acknowledgements

More than two years of my Master of Science by research study has come to the end. I would like to gift this dissertation to all my beloved supervisors, families, colleagues and friends.

First, I would like to thank my supervisor Dr. Maria Ana Cataluna for her great guidance, help and patience. I thank her for receiving me as her Msc by Research student so I had the chance to study abroad for the first time in my life. She supported me greatly on publishing papers on journals and conferences as well as this dissertation. The conversations between us not only guided me in my studies but also improved my English significantly.

I would also like to thank my co-supervisor Dr. Ying Ding and his kind families. It was him that taught me the knowledge of semiconductor mode-locking lasers and guided me through all the experimental process. I really appreciate his help to my daily life abroad and encouragements while I had difficulties in studies or in my life. His help made me feel warm and not that homesick while I was alone in a foreign country.

My many special thanks go to my former supervisor Professor Jiaoqing Pan in Institute of Semiconductors, Chinese Academy of Sciences, who introduced me to Maria Ana and Ying to study in University of Dundee. He opened me the door to the semiconductor lasers' world and played a crucial role in my initial training to become a researcher. Many thanks to him for taking care of me and helping me in my studies and life, no matter I was in China or abroad.

I would like to express my deep gratitude to my aunt Mrs. Gong for supporting me and encouraging me to study abroad. I thank her for being deeply concerned about my health, mentality, study and daily life while I was far away from home. She answered me many questions about problems in my daily life. I would like to thank her for telling me and keeping showing me how to be a positive, active, nice and generous person.

Many thanks go to Mr. Huolei Wang in Institute of Semiconductors, Chinese Academy of Sciences for the successful collaboration on those laser chips. His good work made us able to go smoothly on our research and had excellent results of semiconductor mode-locking lasers.

Thank Professor Weixi Chen in Peking University for her kind suggestions to my dissertation writing.

I would like to thank David Bajek, Stephanie White and Adam Forrest for their help in my experiments. It was very pleasant to study and work with them. They also helped me a lot in my life, introduced me the western culture and had fun together.

I would also like to thank my hospitable and nice colleagues in our office. They are Craig, Phil, Yuri, Stella, Lauren and Steve. I had a really relaxing and happy time there with them.

At last, a special word of thanks goes to my parents. Their selfless support and dedication to me gives me endless motivation.

Content

1. Introduction

1.1 Semiconductor lasers

Semiconductor lasers are the active laser medium made of semiconductor materials. There is a type of important electronically pumped semiconductor laser which is known as semiconductor laser diode (LD). There are more than ten kinds of semiconductor materials that can be used as their work substance, such as indium phosphide (InP), gallium arsenide (GaAs), gallium nitride (GaN) and so on. At the beginning, early semiconductor LDs were only able to work at very low temperature such as 77K. After many years of developments, they can now keep long time working under room temperature. Their structures also developed from homojunction to single heterojunction, double heterojunction, quantum well (single and multiple quantum wells) and other forms. The fast development of semiconductor LDs was from 1960s. The advantages of semiconductor LDs are small volume, light weight, low cost, selectable wavelength, and so on, which make them widely used throughout optical communications, clinical applications, and military. The high power semiconductor lasers have made the most prominent developments and usage.

1.1.1 Principles of laser generation

Semiconductor laser is a coherent radiation source. In order to make it generate laser light, there are three basic requirements:

(1) Population inversion and optical gain: first, establishing the population inversion in the laser medium (active region). In order to achieve this, the occupation probability of the conduction band states must be higher than the occupation probability of the valence band states. This can be achieved by applying forward current to the p(i)n junction (homojuction or heterojunction). In doing so, the electrons in the conduction band can undergo stimulated transitions from the

conduction band state to the valence band state triggered by photons generated from spontaneous emission, and then to generate stimulated emission, i.e., contributing to optical gain. We should note that the optical gain may be less than zero. The lowest injection current density for letting the laser medium become transparent is called transparency current density. Above the transparency current density, the optical gain becomes positive, that is, the rate of stimulated emission is larger than the rate of absorption, or the net optical gain is greater than zero.

(2) Resonant cavity: to obtain the effective stimulated coherent radiation, the radiation must be stimulated and amplified during the propagation in the cavity formed by the two mirrors. The laser resonator or cavity is composed of the natural cleavage planes of the semiconductor crystal or artificial grating. For the F-P cavity (Fabry-Perot cavity) semiconductor laser crystal can easily use two [110] planes (facets) and p-n junction plane perpendicular to the natural cleavage planes as waveguide to constitute an F-P cavity. In this case, usually a highly reflective film is coated on one side and anti-reflective film on another side of the LDs, so the laser emission can come out mostly from one side of the laser.

(3) Threshold conditions: in order to form a stable oscillator, the laser medium must be able to provide enough modal gain (material gain multiplied by optical confinement factor) to compensate the light losses caused by the internal loss (i.e. waveguide propagation loss and free carrier absorption loss) and the cavity loss from the facets of the laser, so the intensity of the optical field in the cavity can be kept increasing during the propagation. The laser output from both facets of the laser can be defined as the cavity loss, which means there is a trade-off between output power and total loss. This requires strong enough current injection which means sufficient gain must be obtained to balance the total loss. The higher the degree of inversion, the greater the resulted gain, which must be met by certain requirements of the threshold current conditions, that is gain is equal to losses during the round trip in the cavity. Once the injected current on the LD is higher than the threshold current, laser with a specific wavelength can be generated in the cavity and emit from the laser facets.

Obviously, from the aspect of materials, a low threshold current can be expected from a LD with a low internal loss.

1.1.2 Threshold current

For an F-P cavity laser, assume the refractive index is n and the reflectivities of the two cavity facets are R_1 and R_2. The gain condition must cover the loss inside the laser at least. [1]

$$R_1 R_2 \exp\left[\frac{i4\pi nL}{\lambda_0}\right] \exp[2(g-\alpha_i)L] = 1 \tag{1.1}$$

λ_0 is the wavelength in vacuum, α_i is the internal loss and g is the gain.

The corresponding threshold gain is:

$$g_{th} = \alpha_i + \frac{1}{2L} \ln \frac{1}{R_1 R_2} \tag{1.2}$$

Increasing the length of the gain section and coating the cavity facet appropriately can bring down the cavity loss and, therefore, reduce threshold current.

1.1.3 Characteristic temperature

As we know, semiconductor devices are sensitive to operation temperature. The threshold current I_{th} increases and the wavelength of the generated laser shifts to longer wavelength as well when the temperature rises. [3, 4] This is because the higher temperature brings more absorption loss, less gain and narrower bandgap. [5, 6]

The relationship between threshold current and characteristic temperature can be shown as:

$$I_{th} = I_{th0} \exp(T/T_0) \tag{1.3}$$

T_0 is the characteristic temperature. The higher T_0 is, the more stable to temperature the laser is.

1.2 Ultrafast lasers

Ultrashort pulse lasers are attractive sources for a number of applications including optical fiber communication, biomedical imaging, high-speed sampling and terahertz (THz) generation. The development of ultrashort optical pulse sources has become a hot research topic in recent years, and picosecond pulse sources have been designed for clock distribution [7], optical fiber radio equipment [8], ultra high speed logic analyzer [9], high-speed clock capture [10], ultrafast signal processing and optical time division multiplexing transmission equipment.

Titanium:sapphire solid-state mode-locked lasers have been widely used as ultrashort optical pulse sources. However, they are bulky and expensive, and controlling the pulse repetition frequency and the electronic synchronization pulse characteristics are relatively complicated. Semiconductor mode-locked lasers have advantages in compactness, weight, energy efficiency and cost. These make them excellent candidates for ultrashort pulse generation. More and more researchers started to put effort in semiconductor mode-locking lasers and significant achievements have been made. The numbers of the published papers about mode-locked semiconductor laser over two decades are shown in Figure 1.1. It shows that semiconductor mode-locked laser research field has been growing in importance.

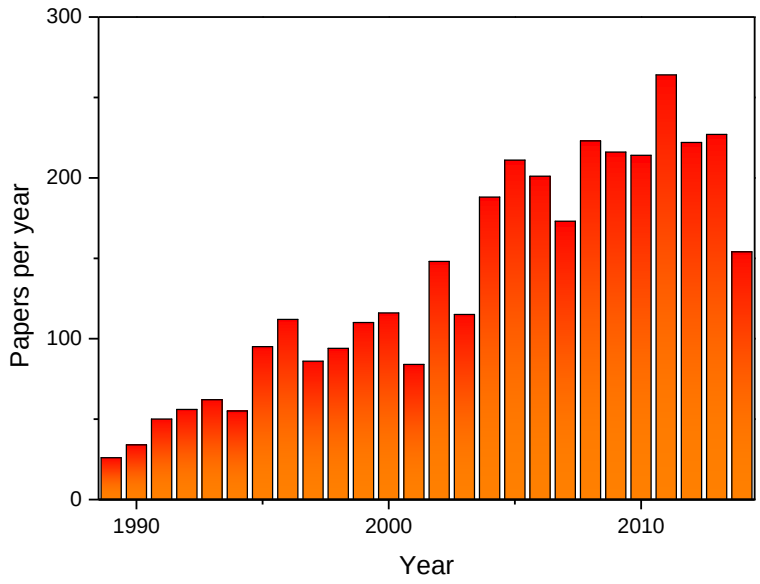

Fig. 1.1 The trends of paper number of mode-locked laser recent twenty years (Data origin, ISI; Key words: “mode-locked” “semiconductor” “lasers”)

The small size, high stability, low cost and direct electrical pumping increases the range of applications of semiconductor mode-locked lasers. Mode-locked semiconductor lasers are particularly interesting for applications in communication systems. These lasers can generate pulses at very high repetition rate and with record-low jitter which are very useful for optical time division multiplexing systems (OTDM), where a mode-locked laser can be used either as a pulse source or in a clock recovery circuit.

Short optical pulses with high peak power generated by the semiconductor mode-locked lasers can also be used to obtain non-linear effects. It is of vital importance for a number of applications, such as multiphoton bio-imaging [11, 12].

1.3 The physics of mode-locked laser diodes (MLLDs)

Pulse generation from mode-locking is achieved through the phase locking of the longitudinal modes of a laser diode by controlling an intracavity gain, loss or phase

element. Methods for producing mode-locking in a laser can be classified as active, passive and hybrid. Active methods typically involve using an external signal to induce a modulation of the intra-cavity light. Passive mode-locking techniques are those that do not require a signal external to the laser to produce pulses, and therefore are widely used in many lasers to generate short pulses.

The basic structure of a typical passively mode-locked semiconductor laser is a two-section device, which includes the gain region and the saturable absorption region, figure 1.2.

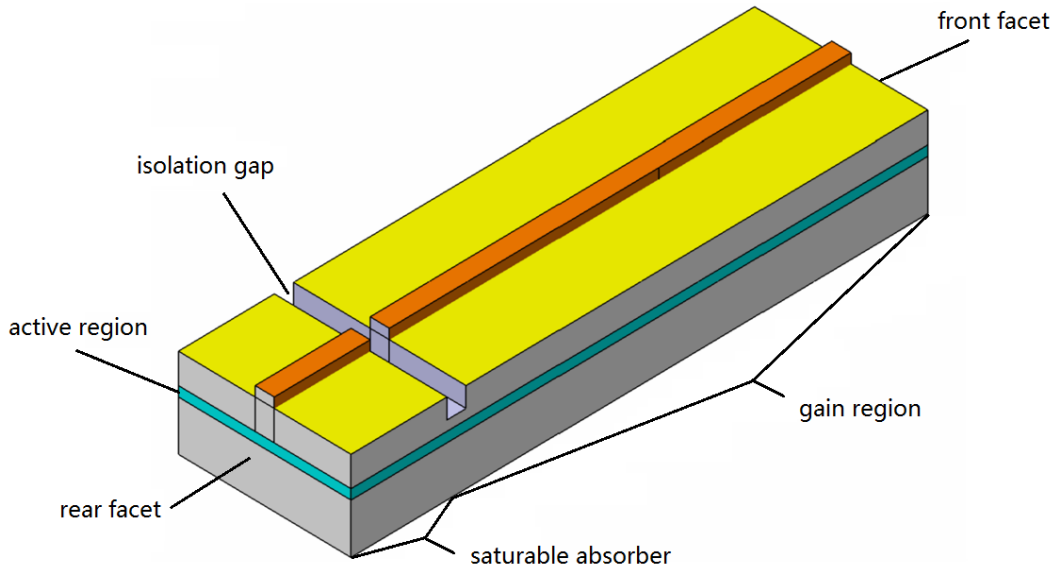

Fig. 1.2 The typical basic structure of a semiconductor laser used in passive mode-locking regime.

The two sections are electrically isolated by an isolation groove. However, the optical waveguide between the two sections is continuous. During the operation, the gain region produces gain by applying a forward current to the gain section, and the saturable absorber is reverse biased, which enables the control of the absorption recovery time. The intensity of the travelling wave inside the laser cavity saturates the absorber section during propagation. The absorber saturates and recovers faster than the gain medium, therefore, creating a short net gain window in which cavity losses

can be compensated, leading to a periodic amplification of the travelling field for the duration of the window openings, thus obtaining a short pulse. This is due to the saturable absorption in a nonlinear absorption medium - the absorption changes with the intensity of the optical field inside the resonant cavity [13]. The optical absorption is quite strong when the optical field is weak. Thus, the transmittance of light is low. The optical absorption of the saturable absorber decreases while the intensity of the optical field increases gradually. When the absorber is saturated, the light can pass through it with relatively low loss. So the higher the optical power, the less loss. The nonlinear saturable absorption characteristic of the saturable absorber can be understood considering the dynamics of electron-hole pairs excited by light. Such electrons and holes are located in the conduction band and valence band respectively, in a quantity that increases with the light intensity. If the light intensity increases to a certain extent, due to the limited density of states for electrons and holes, the available sates that can be occupied are saturated, and no more photons can be absorbed. The optical absorption decreases with the increasing light intensity. So, high intensity laser, generated by high gain laser, can saturate the absorber. The transmittance of strong light field is larger than the one of weak field, only a small portion is absorbed by the absorber. Before the mode-locking, every time the pulse passes through the absorber, the proportion of the strong signal to weak signal increases. After multiple roundtrips inside the cavity, the front edge of the pulse becomes steeper and steeper. The peak part can pass the absorber smoothly and make the pulse become sharper and sharper. The schematic diagram of the loss and gain dynamics that lead to pulse generation is shown in Figure 1.3.

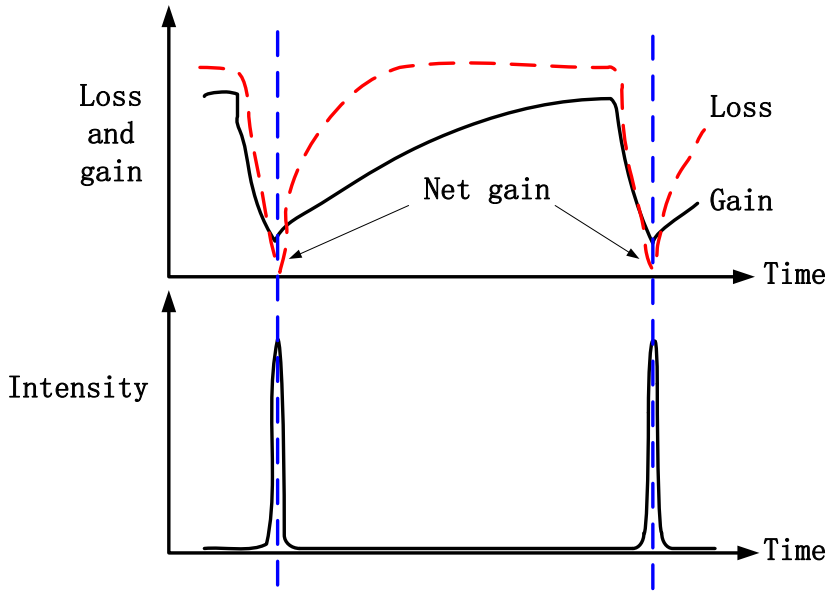

Fig. 1.3 The schematic diagram of the loss and gain dynamics that lead to pulse generation [14]

Initially, the laser output is generated when the threshold current is reached. Under the selecting effect of the saturable absorber, only the high-gain center wavelength and sideband modes are left. After the multiple amplification by the gain section and absorption by the absorber section, more sideband modes are generated. Finally, all longitudinal modes in the gain width above the gain threshold oscillate and couple with each other. So it generates a series of pulses with 2nL/c period or c/2nL pulse repetition rate, where c is the speed of light, L is the laser length and n is the refractive index of the laser. Multi-longitudinal modes in the cavity are eventually formed in unison with a fixed phase relationship in the end. Lasers under this working mode are called mode-locked lasers.

1.4 Mode-locked lasers in the 750 – 770 nm region: state of the art

To make semiconductor mode-locking lasers better ultrashort pulse sources, minimizing the pulse width and maximizing the peak power are the goal of most researches. Different wavebands have been demonstrated in this context, ranging from

1.26 μm, based on a combination of InAs/GaAs picosecond quantum dot laser and amplifier [15], down to the near-infrared at 783 nm, which was demonstrated with a picosecond all-semiconductor master-oscillator power-amplifier based on a GaAs quantum-well (QW) structure [16]. In order to achieve pulses in 750 nm – 770 nm, there are also previous works that used fiber-amplified infrared gain-switched laser diodes with additional second-harmonic generation schemes to convert their infrared output into the 774 nm [17] or 766 nm [18] spectral wavebands. The possibility of engineering the bandgap of semiconductor materials affords significant spectral flexibility, with the potential to enable direct generation of ultrashort pulses in the red. [19,20] The very recent demonstration of red mode-locked vertical external-cavity surface emitting lasers (VECSELs) has shown it is possible to generate visible ultrashort pulses directly from optically pumped semiconductor lasers, with pulse durations of about 5 ps [19] or 250 fs, [20] for pulse repetition rates of 973MHz or 836 MHz, respectively. Up until now, only one class of semiconductor monolithic mode-locked lasers has been demonstrated across the visible spectral region - picosecond InGaN edge-emitting two-section lasers, emitting in the blue-violet range. [21]

In this dissertation, passively mode-locked AlGaAs multi-quantum-well (MQW) edge emitting laser diodes with central wavelength of 766 nm and 752 nm are reported. Importantly, the latter also represents the shortest wavelength ever to be generated directly by an ultrafast edge emitting laser in the red to near-infrared spectral waveband.

1.5 Research trends of semiconductor mode-locking laser

While the research on laser goes deeper, people start to attach importance to not only more diverse wavelengths but also better performance in time domain. So far, the research trends include the several aspects below.

(1) High repetition frequency. High repetition frequency is of vital importance for some applications, such as multi-photon bio-imaging. High repetition frequency pulse

source can improve the signal to noise ratio and sample rate of the signal effectively. Pulses with high repetition frequency can be used in large-capacity telecommunication systems [22], optical switching device [23], optical clock and high speed electro-optic sampling and other fields as an information carrier.

(2) High power. In many applications, high power of single pulse or high average power is in high demand. In this case, single or multiple amplification stages are typically used to get enough power from semiconductor lasers. This makes the whole system more complicated. So high power laser from semiconductor laser sources can be directly used in bio-imaging, processing field and so forth or at least decrease the amount of amplifiers needed.

(3) Shorter pulse width. Because of the limit of gain medium bandwidth of semiconductor lasers, the pulse widths of semiconductor lasers are typically wider than that of solid-state mode-locked lasers. It is possible to narrow the pulse width of semiconductor laser with broader gain media. This is of vital importance for the development and application of semiconductor mode-locking lasers.

(4) Research on mode-locking devices and materials. The development of material science also improves the development of semiconductor mode-locking laser device. In the recent years, new materials, such as graphene, are used to realize mode-locking in lasers.

(5) Research on mode-locking mechanism. It is a complicated process to generate pulses from mode-locked laser. Much research has been put on the mechanism. Many new phenomena were found out, which also improve the performance of the lasers.

1.6 Thesis outline

In this thesis, the results achieved with 750-770 nm mode-locked laser diodes are presented, focusing more on their characterization. In chapter 2, the experimental methods including the test setup and the devices, including the autocorrelator, which is key for characterization of the pulses are described. In chapters 3 and 4, the test results of the 760 nm and 750 nm laser diodes respectively including the P-I curves,

optical spectra, repetition frequency spectra, autocorrelation traces of the pulses and analysis of the results are presented. The work is summarized in chapter 5.

1.7 References

[1] Jianping Jiang, "Semiconductor Lasers," *Publishing House of Electronics Industry*, 2000.

[2] I. Schnitzer, E. Yablonovitch, C. Caneau et al., "Ultrahigh spontaneous emission quantum efficiency, 99.7% internally and 72% externally, from AlGaAs/GaAs/AlGaAs double heterostructures," *Applied Physics Letters*, vol. 62, no. 2, pp. 131-133, 1993.

[3] K. Takeshi, N. Kouji, K. Masahiko et al., "A 1.3-μm GaInNAs/GaAs Single-Quantum-Well Laser Diode with a High Characteristic Temperature over 200 K," *Japanese Journal of Applied Physics*, vol. 39, no. 2A, pp. L86, 2000.

[4] K. Mukai, Y. Nakata, K. Otsubo et al., "High characteristic temperature of near-1.3-μm InGaAs/GaAs quantum-dot lasers at room temperature," *Applied Physics Letters*, vol. 76, no. 23, pp. 3349-3351, 2000.

[5] E. Z. Alexey, M. U. Victor, E. Anton Yu et al., "Negative Characteristic Temperature of InGaAs Quantum Dot Injection Laser," *Japanese Journal of Applied Physics*, vol. 36, no. 6S, pp. 4216, 1997.

[6] S.-H. Park, and Y.-T. Moon, "Temperature characteristics of spontaneous emission and optical gain in blue InGaN/GaN quantum well structures," *Journal of Applied Physics*, vol. 114, no. 8, pp. 083107, 2013.

[7] Delfyett, P.J., D.H. Hartman, and S.Z. Ahmad, "Optical clock distribution using a mode-locked semiconductor laser diode system," *Lightwave Technology, Journal of*, 1991. 9(12): p. 1646-1649.

[8] Vieira, A.J.C., et al., "A mode-locked microchip laser optical transmitter for fiber radio," *Microwave Theory and Techniques, IEEE Transactions on*, 2001. 49(10): p. 1882-1887.

[9] Vlachos, K., et al., "Ultrafast time-domain technology and its application in

all-optical signal processing," *Lightwave Technology, Journal of*, 2003. 21(9): p. 1857-1868.

[10] Ohno, T., et al., "Recovery of 160 GHz optical clock from 160 Gbit/s data stream using modelocked laser diode," *Electronics Letters*, 2004. 40(4): p. 265-267.

[11] M. Kuramoto, N. Kitajima, H. Guo, Y. Furushima, M. Ikeda, and H. Yokoyama, *Opt. Lett*. 32(18), 2726–2728, 2007.

[12] Y. Ding, R. Aviles-Espinosa, M. A. Cataluna, D. Nikitichev, M. Ruiz, M. Tran, Y. Robert, A. Kapsalis, H. Simos, C. Mesaritakis, T. Xu, P. Bardella, M. Rossetti, I. Krestnikov, D. Livshits, I. Montrosset, D. Syvridis, M. Krakowski, P. Loza-Alvarez, and E. Rafailov, *Opt. Express* 20(13), 14308–14320, 2012.

[13] M. Haiml, R. Grange, and U. Keller, "Optical characterization of semiconductor saturable absorbers," *Applied Physics B*, vol. 79, no. 3, pp. 331-339, 2004/08/01, 2004.

[14] E. U. Rafailov, M. A. Cataluna, W. Sibbett, "Mode-locked quantum-dot lasers," *nature photonics*, Vol. 1, July 2007.

[15] Y. Ding, R. Aviles-Espinosa, M. A. Cataluna, D. Nikitichev, M. Ruiz, M. Tran, Y. Robert, A. Kapsalis, H. Simos, C. Mesaritakis, T. Xu, P. Bardella, M. Rossetti, I. Krestnikov, D. Livshits, I. Montrosset, D. Syvridis, M. Krakowski, P. Loza-Alvarez, and E. Rafailov, "High peak-power picosecond pulse generation at 1.26 μm using a quantum-dot-based external-cavity mode-locked laser and tapered optical amplifier," *Opt. Express* 20(13), 14308–14320, 2012.

[16] M. Kuramoto, N. Kitajima, H. Guo, Y. Furushima, M. Ikeda, and H. Yokoyama, "Two-photon fluorescence bioimaging with an all-semiconductor laser picosecond pulse source," *Opt. Lett*. 32(18), 2726–2728, 2007.

[17] H. Yokoyama, H. Guo, T. Yoda, K. Takashima, K.-i. Sato, H. Taniguchi, and H. Ito, "Two-photon bioimaging with picosecond optical pulses from a semiconductor laser," *Opt. Express* 14(8), 3467–3471, 2006.

[18] T. Schoenau, T. Siebert, R. Haertel, T. Eckhardt, D. Klemme, K. Lauristen, and R. Erdmann, "Pulsed picoseconds 766 nm laser source operating between 1-80 MHz

with automatic pump power management,” in *Nonlinear Frequency Generation and Conversion: Materials, Devices, and Applications XII* (SPIE, San Francisco, CA, 2013.

[19] S. Ranta, A. Harkonen, T. Leinonen, L. Orsila, J. Lyytikainen, G. Steinmeyer, and M. Guina, *Opt. Lett*. 38(13), 2289–2291, 2013.

[20] R. Bek, H. Kahle, T. Schwarzback, M. Jetter, and P. Michler, *Appl. Phys. Lett*. 103(24), 242101, 2013.

[21] P. P. Vasilev, A. B. Sergeev, I. V. Smetanin, T. Weig, U. T. Schwarz, L. Sulmoni, J. Dorsaz, J. M. Lamy, J. F. Carlin, N. Grandjean, X. Zeng, T. Stadelmann, S. Grossmann, A. C. Hoogerwerf, and D. L. Boiko, *Appl. Phys. Lett*. 102(12), 121115, 2013.

[22] L. F. Mollenauer, P. V. Mamyshev, J. Gripp et al., “Demonstration of massive wavelength-division multiplexing over transoceanic distances by use of dispersion-managed solitons,” *Optics Letters*, vol. 25, no. 10, pp. 704-706, 2000/05/15, 2000.

[23] D. A. B. Miller, “Optical interconnects to silicon,” *Selected Topics in Quantum Electronics, IEEE Journal of*, vol. 6, no. 6, pp. 1312-1317, 2000.

2. Experimental methods

2.1 Experimental setup

The schematic diagram of the experimental arrangement is shown in Fig. 2.1.

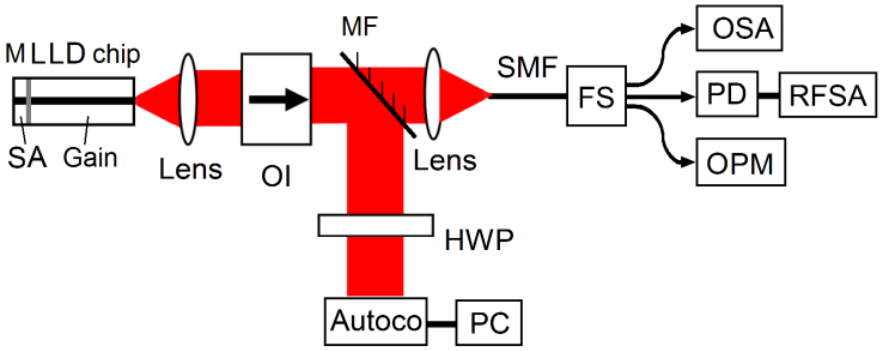

Fig. 2.1 Experimental setup used for the characterization of the mode-locking laser diodes (MLLD), comprising a gain and saturable absorber (SA). Legend - OI: optical isolator; MF: mirror flipper; HWP: half wave plate; SMF: single-mode fiber; FS: fiber splitter; OSA: optical spectrum analyzer; PD: photo detector; RFSA: RF spectrum analyzer; OPM: fiber optical power meter; Autoco: autocorrelator.

In the experimental work, the temperature of the laser diode has been fixed at 10 ℃, with a thermoelectric temperature controller. The Newport Model 6100 was used as our current driver and temperature controller. We use Agilent E3647 as our power supply to provide reverse bias. After collimation, an optical isolator is used to prevent reflections back into the laser. The output of the MLLD was coupled into a single mode fiber splitter. Then the laser was guided to an optical power meter, an RF spectrum analyzer and an optical spectrum analyser (OSA) for the characterization and monitoring. We use an Agilent RF analyser and an Anritsu MS9710C as our OSA. An APE Pulse Check autocorrelator based on second harmonic generation was used to

measure the pulse duration. A preliminary laser beam profiling and wavefront study suggests that the MLLD is operating under a single fundamental mode regime. The output average power of MLLD had been measured by Thorlabs PM100D and an integrating sphere power meter, placed between the collimating lens and an optical isolator. Fig. 2.2 is the photo of the main experimental setup which shows the chip and the optical paths. Fig. 2.3 is a close-up of the chip.

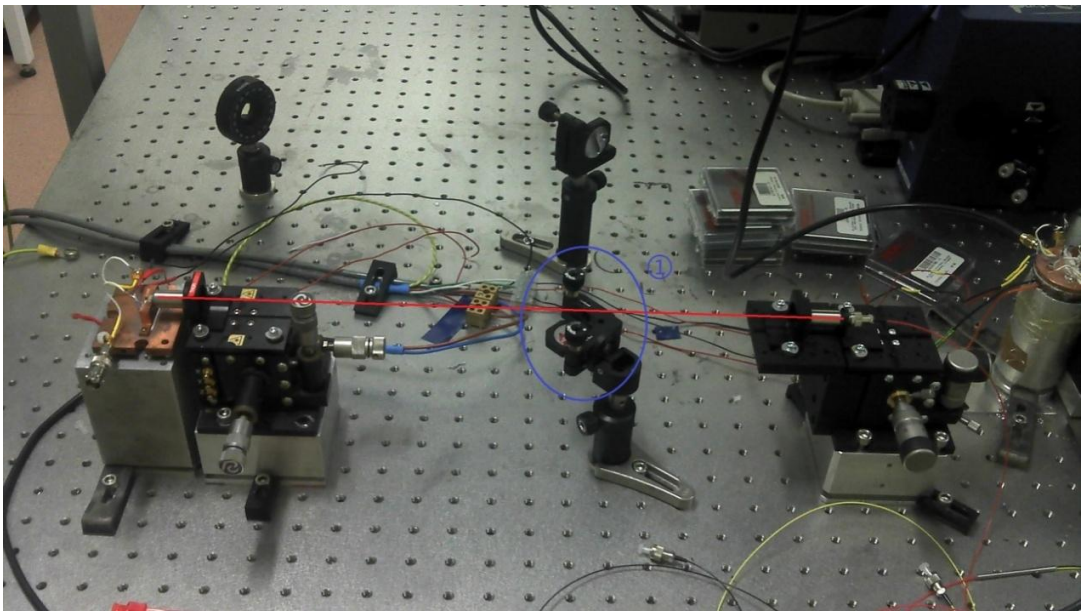

Fig. 2.2 Photo of the experimental arrangement

The red line illustrates the beam path of the laser. The mirror in the blue circle marked with ① is the mirror flipper which can guide the beam to the autocorrelator, when it is lifted up.

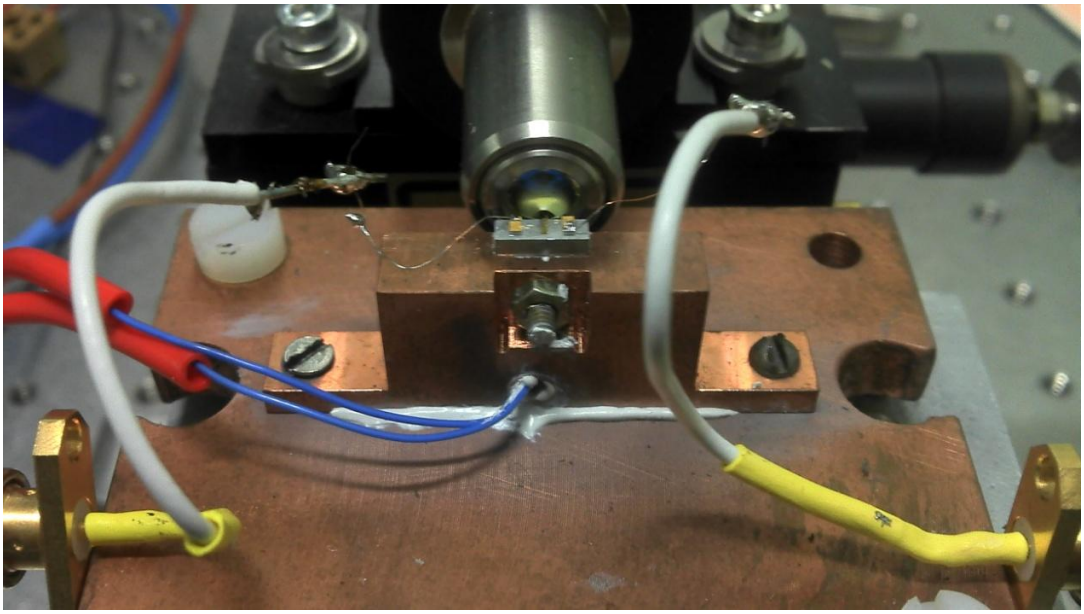

Fig. 2.3 Close-up of the chip

Fig. 2.3. shows how the chip is mounted. We can see the two cables connected to the gain section and the absorption section respectively. The thermistor is in the hole which is right under the chip. The divergence angle is large so the collimation lens is quite close to the emitting facet of the chip.

2.2 Radio frequency spectrum analyzer

We use an Agilent RF analyser in our experiment to help to identify if the laser is mode-locked and check the repetition frequency of the pulses, as this instrument transforms a time-domain signal into a frequency spectrum. The RF analyser is based on a narrow band receiver for measuring high frequency signals. Before being characterized by the analyser, the laser was coupled into a fiber connected to a high-speed photo detector, in which the optical signal is transformed into an electrical signal that can be detected by the analyser. In the RF analyser, the frequency of the receiver keeps sweeping repetitively over the desired range of frequencies. An attenuator is placed right after the input, so that signal's intensity is decreased. Then the signal's high frequency part is blocked after passing through a low-pass filter. After that, a mixer mixes the signal with another signal from a local oscillator. Two

original signals and their harmonics and the sums and differences of the original frequencies and their harmonics come out from the non-linear mixer. Only the signals that are in the pass band of the intermediate frequency filter are then sent to an amplifier. The resolution bandwidth is determined by the bandwidth of the filter. A narrower bandwidth enables higher resolution but decreases the sweep rate which also means increasing the sweep time.

As mentioned before, when the laser is mode-locked, a train of pulses is generated with a certain pulse repetition rate. In this case, we shall see a single stable sharp peak on the screen of the RF analyser, corresponding to this frequency. It can also help us judge the performance of the mode-locking in the laser and to see if it is stable.

2.3 Autocorrelator

An autocorrelation method is used to measure the pulse duration of the pulses generated by these lasers, as their typical duration (a few picoseconds) is too short to be observed directly by a standard photodetector and oscilloscope. The optical layout of an autocorrelator is based on a Michelson interferometer, which introduces a relative delay between a pulse and its replica. The two beams are then focused into a nonlinear crystal, generating a second-harmonic signal which is then detected as the delay is varied, resulting in a second-order autocorrelation, which can provide an indication of the pulse duration.

There are two main autocorrelation methods: collinear and non-collinear. For the collinear method, shown in Fig. 2.4, the beam is divided into two after passing the beam splitter. After that, the two beams are reflected by two mirrors respectively and hit the crystal coaxially. The optical structure of autocorrelator is mainly formed by the beam splitter, mirrors (with translation stage), crystal, filters and photomultiplier tube and so on. The beam splitter, crystal, filters and photomultiplier tube are chosen mainly based on the matching of the laser wavelength and the second harmonic wavelength.

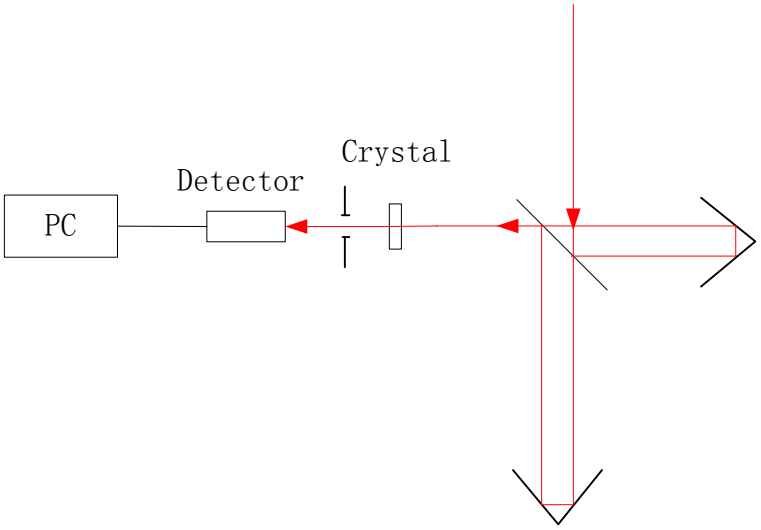

Fig. 2.4 Collinear autocorrelation schematic.

By adjusting the position of the retroreflector (which consists of two mirrors right-angled to each other), the two beams can then have different optical paths. If we change the position of the retroreflector continuously, it will form a pulse sequence that scans the other, which forms a trace of the autocorrelation function. When the two beams hit the crystal with a matching orientation at the same time, the second harmonic will be generated. The harmonic optical signal is only related to the product of the two input beams. The generated second harmonic is received and recorded by the photomultiplier tube (PMT).

In this work, the non-collinear measurement method is used. As shown in Fig. 2.5, in this method, the two beams are not coaxial. They are focused on the crystal after passing a lens. The second harmonic is acquired by adjusting the orientation and length of the light paths, received and recorded by the PMT like in the collinear method too. This method results in a background-free autocorrelation.

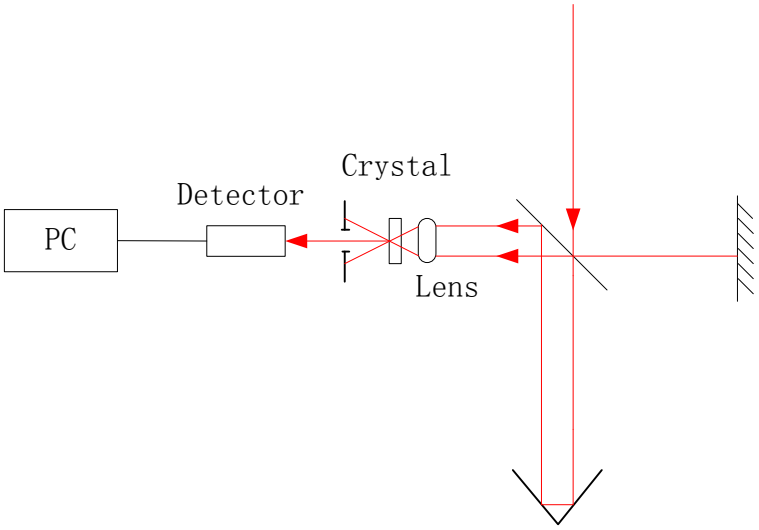

Fig. 2.5 Layout of a non-collinear autocorrelator.

It is easy to show that an autocorrelator converts a length measurement into a time measurement. These instruments measure the autocorrelation of the pulse rather than the pulse itself. The full width at half maximum (FWHM) of the autocorrelation is directly related to the pulse width.

In the experimental work, the APE Pulse Check autocorrelator is used to characterize the pulses. As shown in Fig. 2.6, after entering the optical assembly at the input aperture, the laser pulse is divided into two parts at the beam splitter. Each part traverses an interferometer arm containing a retroreflector. One of the retroreflectors is mounted on a special linear translation stage that can change the length of one interferometer arm in a continuous fashion. After traversing the beam splitter, the two beams are then focused by a lens and overlapped in a nonlinear optical crystal. The second harmonic radiation generated in the nonlinear crystal is then detected by a filtered photomultiplier tube.

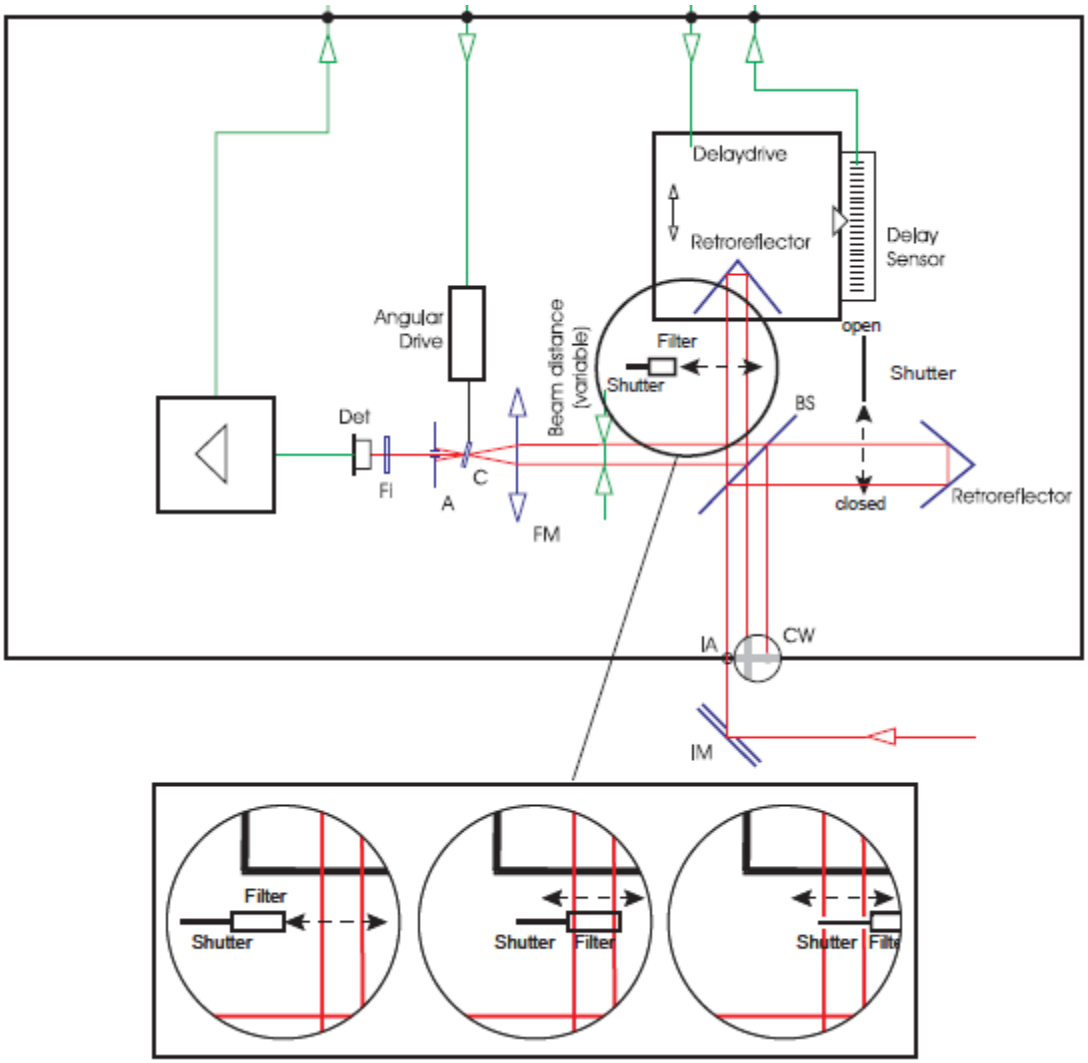

Fig. 2.6 The schematic principal optical layout [1]

The vibration of the retroreflector causes the length of the light path to continuously change which means the transmitted pulse train is delayed (or advanced) compared to the reference (zero delay) position. The photomultiplier output is connected to the APE Pulse Check display unit, which shows the resulting autocorrelation. The rapid and repetitive scanning enables real-time measurements of the autocorrelation function of the pulses.

It is important to note that the autocorrelation trace is not the pulse itself. So a factor is needed to be multiplied to get the width of the pulse from the width of the autocorrelation. There are several kinds of fits that are usually used to fit the trace of the autocorrelation function, assuming pulse shapes such as Gaussian, hyperbolic

secant squared ($sech^2$) and Lorentzian. Each kind of fit has its own factor that represents the relationship between the FWHM of the function and the real pulse width.

2.4 References

[1] APE. PulseCheck manual. MagicSM#115279

3. 760-nm Mode-Locked Laser Diodes

3.1 Device structure and fabrication

There are two types of multi-quantum-well (MQW) structures for our 760-nm mode-locked laser diodes, shown by Fig. 3.1 and Fig. 3.2, below,. The structure CCS-1124 has 5 quantum wells while CCS-1196 has 3 quantum wells instead.

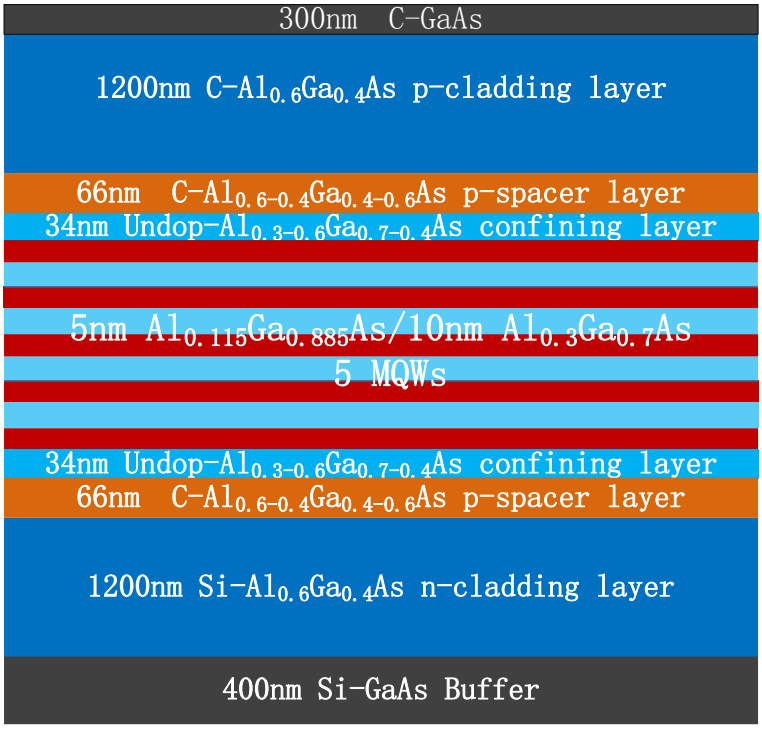

Fig. 3.1 Material structure of CCS-1124

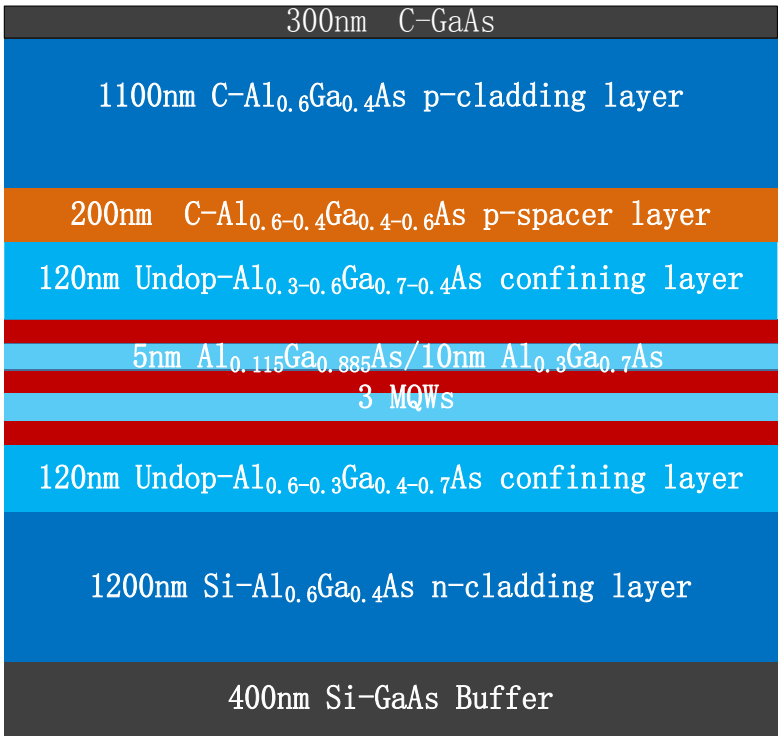

Fig. 3.2 Material structure of CCS-1196

For example, the CCS-1196 material structure, based on AlGaAs multi-quantum-well graded-index separate–confinement-heterostructure, was grown on a heavily n-doped GaAs substrate via Metal Organic Chemical Vapor Deposition (MOCVD) using only one step growth. First, the 1.2-μm-thick Si-doped $Al_{0.6}Ga_{0.4}As$ n-cladding layer was grown, followed by the 0.12-μm-thick undoped linearly compositional-graded $Al_{0.6\text{-}0.3}Ga_{0.4\text{-}0.7}As$ confining layer. The active region was subsequently grown, consisting of three 5-nm-thick $Al_{0.115}Ga_{0.885}As$ quantum wells separated by two 10-nm-thick $Al_{0.25}Ga_{0.75}As$ barrier layers. A 0.12-μm-thick undoped $Al_{0.3\text{-}0.6}Ga_{0.7\text{-}0.4}As$ confining layer was grown atop the active region, followed by a 0.2-μm-thick C-doped linearly compositional-graded $Al_{0.6\text{-}0.4}Ga_{0.4\text{-}0.6}As$ p-spacer layer. Finally, a 1.1-μm-thick C-doped $Al_{0.6}Ga_{0.4}As$ p-cladding layer and 0.3-μm-thick GaAs p^+-contact layer were grown. To address the challenge inherent to the high concentration of aluminium, the growth temperature was kept at relatively high values, with the aim of minimizing the creation of deep-level defects which act as centers of non-radiative recombination. [1] Accordingly, the growth temperature for the GaAs

buffer layer was 754 ℃ and 830 ℃ for the $Al_{0.6}Ga_{0.4}As$ cladding layer, while the other layers were grown at 750 ℃. The confinement factor was calculated to be 0.058.

For both structures, a ridge waveguide material having a width of 3.7 μm to a depth of 1μm was fabricated by means of conventional lithography and inductively coupled plasma (ICP), and was defined by dry etching. A silicon dioxide insulating layer by plasma-enhanced chemical vapor deposition (PECVD) was added. Ti / Au p-metal contacts and Au / Ge / Ni n-contacts were deposited after that. An illustrative diagram of the mode-locked monolithic laser is shown in Fig. 3.3. Two-section lasers with two different cavity lengths were produced: one with a total length of 1815 μm, comprising a 1728 μm long gain section and a 72 μm long saturable absorber. The other type of chips has a total length of 1515 μm, consisting of a 1440 μm long gain section and a 60 μm long saturable absorber. Both lasers have a similar absorber-to-total-length ratio of around 4%. Electrical isolation between the gain and the absorber electrodes is reached by a 15-μm-wide and 350-nm-deep gap in the contact layer by wet etching. The front and rear facets were coated, exhibiting reflectivities of 13.6% and 93.9%, respectively. The chips were mounted epilayer-up on copper heat sinks. The wafer growth, laser processing and mounting were carried out at the Institute of Semiconductors (Chinese Academy of Sciences) and at Beijing University of Technology.

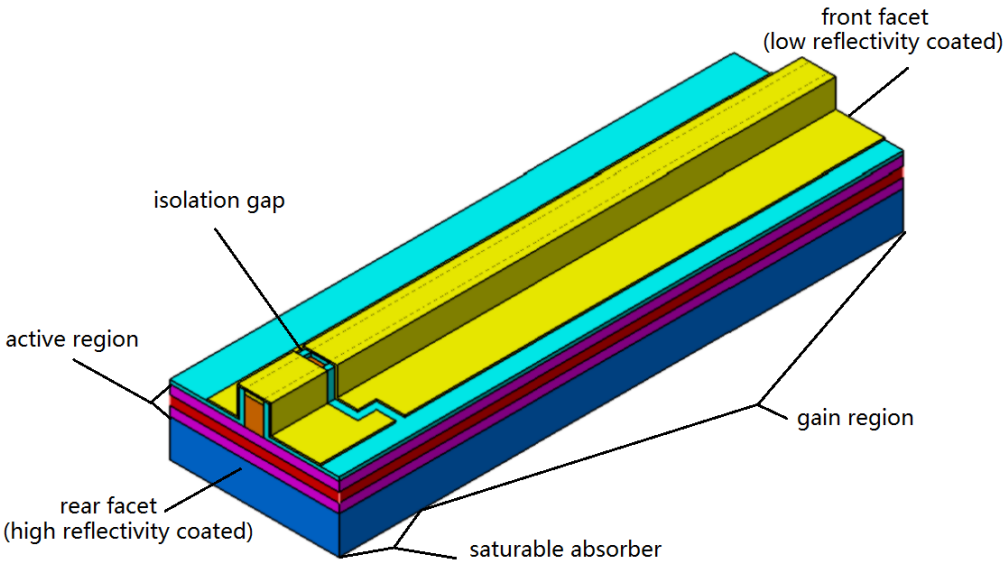

Fig. 3.3 Schematic of the monolithic GaAs-AlGaAs mode-locked laser (not to scale).

3.2 Experimental results

The Table 3.1 lists all the 760-nm MLLD chips that were fabricated. We have eight groups of chips in total, two types of reflectivity, two different material structures and two cavity lengths. The chips identified in red have been tested at Dundee.

Table 3.1 List of all the 760-nm MLLD chips

	AR 6.6%			AR 15%		
CCS-1124 1.8mm	2-1	2-2		**2-1**	**2-2**	2-3
CCS-1196 1.8mm	**3-1**	**3-2**	3-3	**3-1**	**3-2**	3-3
CCS-1124 1.5mm	5-1	5-2	5-3	5-1	5-2	5-3
CCS-1196 1.5mm	6-1	6-2	6-3	**6-1**	6-2	6-3

The following power and voltage characteristics as a function of current (P-I-V curves) were measured by Mr. Huolei Wang, a PhD student in the Institute of Semiconductors, Chinese Academy of Sciences. The P-I-V curves of the 6.6% and 15% AR CCS-1196 1.8 mm long chips were acquired under pulsed input current and continuous current. Both the gain and the absorber section were forward biased. The pulsed current was delivered in pulses of 10 μs and a duty cycle of 1%. Unlike continuous current, this pulsed current mode leads to minimal thermal effects due to Joule heating associated with the forward bias.

The results are shown in Fig. 3.4 to Fig. 3.7.

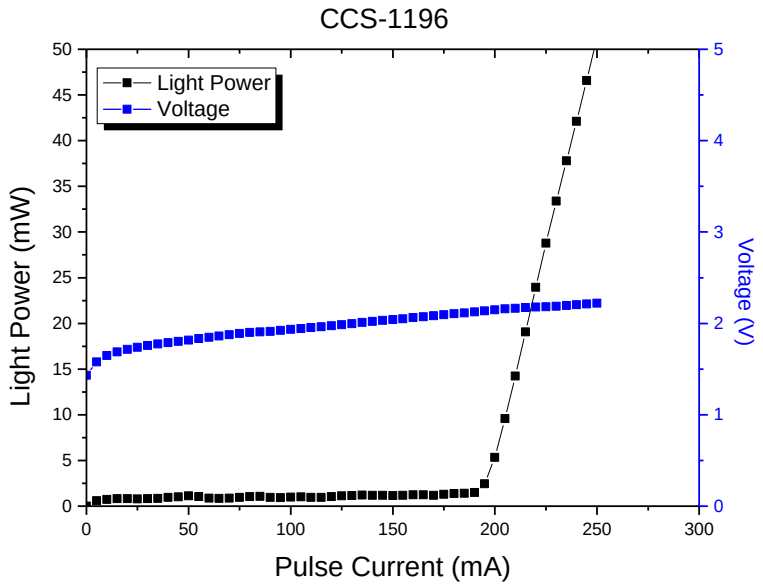

Fig. 3.4 P-I-V curve of CCS-1196 (AR 6.6%) under pulsed current

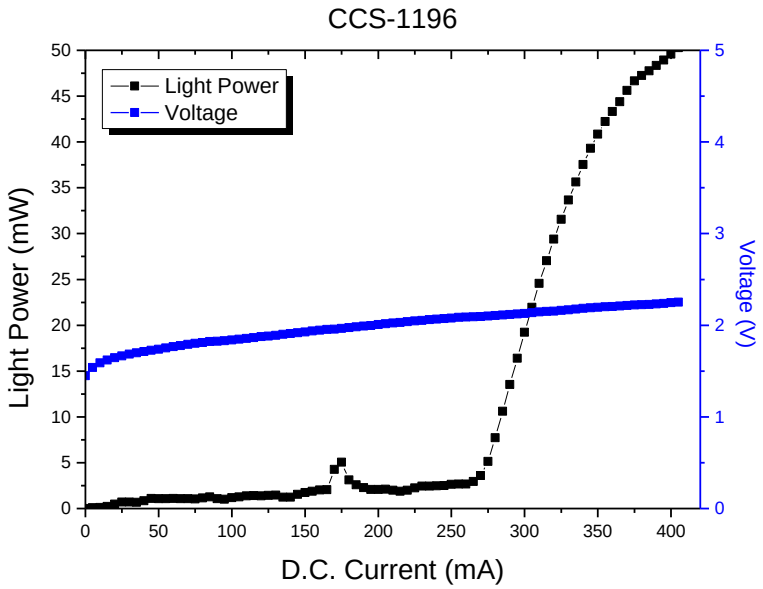

Fig. 3.5 P-I-V curve of CCS-1196 (AR 6.6%) under continuous current

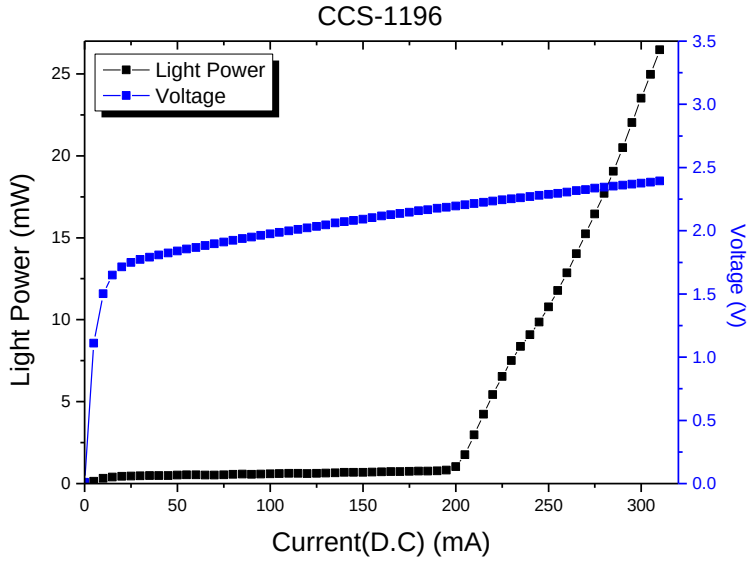

Fig. 3.6 P-I-V curve of CCS-1196 (AR 15%) under pulsed current

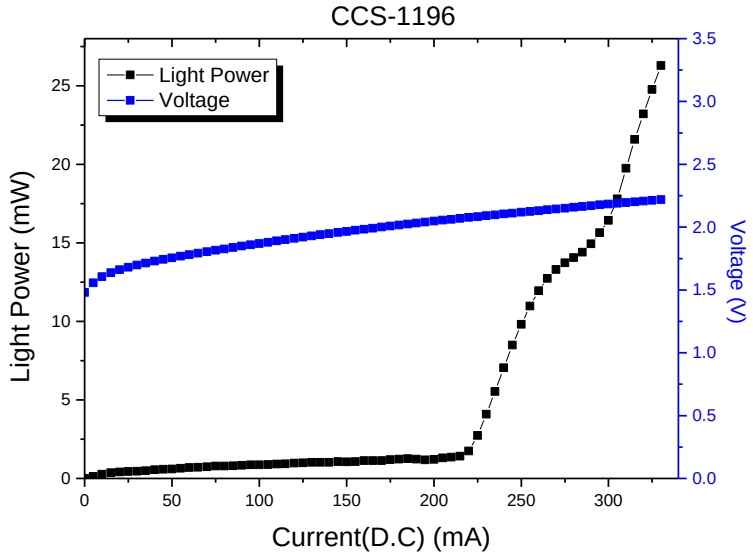

Fig. 3.7 P-I-V curve of CCS-1196 (AR 15%) under continuous current

A comparison between P-I-V curves in pulsed and continuous current modes show that the thermal effects of continuous biasing lead to an increase in threshold current and thermal rollover, which is stronger for the case of the CCS-1196 (6%). This can be explained by increase in the active region temperature due to continuous biasing, which leads to increase in threshold current as explained in section 1.1.3.

From these curves, we can find that, under both pulsed and continuous currents, the chips with 6.6% reflectivity have higher output power than the chips with 15% reflectivity and the threshold current of the lasers with higher reflectivity is lower than the one with lower reflectivity. This is expected, as can be observed in the threshold current and gain expressions in section 1.1.2.

However, it was found that the chips with 6.6% reflectivity were not mode-locked under any conditions of current and reverse bias. It seems that such reflectivity could be too low for mode-locking. With higher front facet reflectivity, the intracavity pulse energy can be higher and saturate the absorber more easily, leading to stable mode-locking. This has been previously shown theoretically [2]. Therefore we abandoned the test on other 6.6% AR chips.

The P-I-V curves of the 6.6% AR CCS-1124 1.8 mm long chips under pulsed input current were tested as well. The results of two chips with exactly the same structure are shown in Fig. 3.8 (a) and (b) respectively.

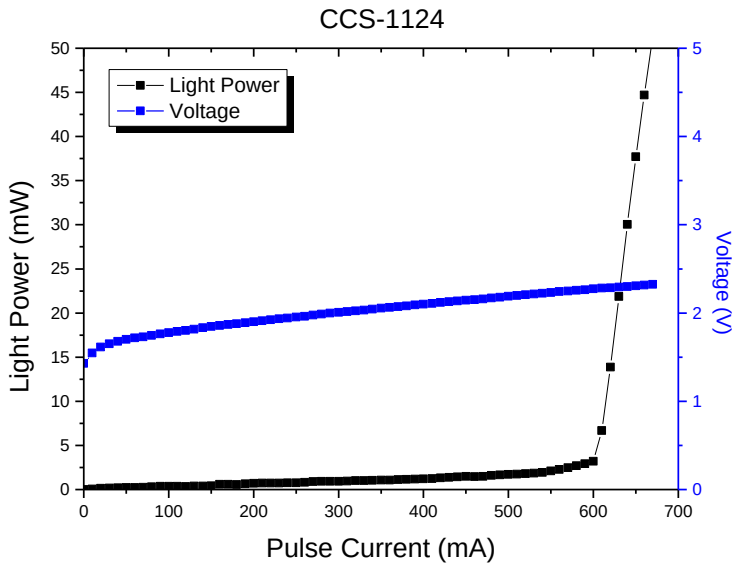

(a)

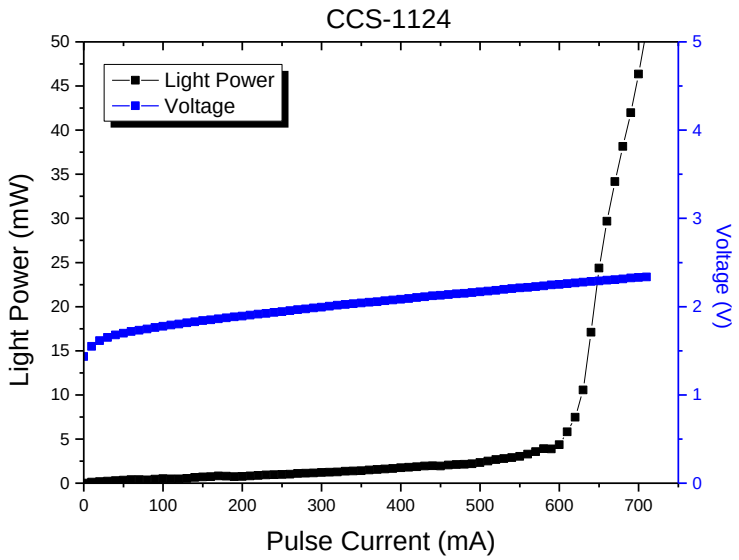

(b)

Fig. 3.8 P-I-V curves under pulsed current of two CCS-1124 (AR 6.6%) devices

Unfortunately, as we tested, the chips with CCS-1124 structure did not display mode-locking. So we did not have more mode-locking results of the AR 6.6% chips beside the P-I-V curves above.

3.2.1 1815 μm long MLLD emitting at 766 nm

As shown in Fig. 3.9, the light-current characteristics of the 1815 μm 766 nm chip were evaluated for different values of reverse bias which was applied to the absorption section of the laser. When the reverse bias increased from -2 V to -3 V, the obvious light power drop can be seen because of the effect of optical absorption.

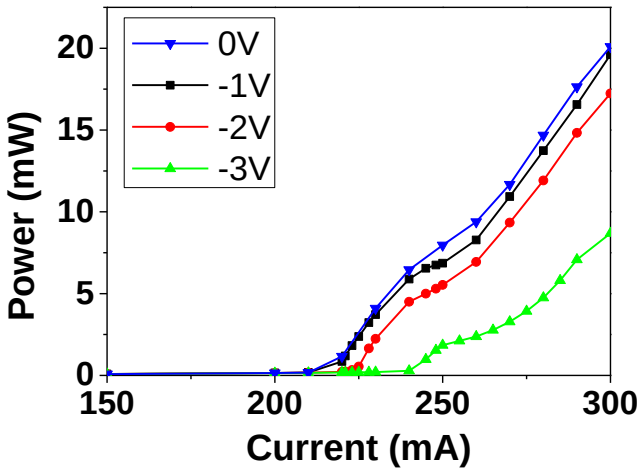

Fig. 3.9 Light-current characteristics of the 1815μm long laser for different reverse-bias conditions at 766 nm.

As we tested, we found the laser can have a stable mode-locking mode when the forward bias currents are higher than 250 mA and the reverse bias is between -2.3 V and -3 V. The value of the reverse bias that makes the laser mode-locked depends on the applied forward bias current. Typical features of the pulsed output are observed under a stable mode-locking regime, shown in Fig. 3.9. The pulse width of the peak is about 5.7 ps with $sech^2$ fit (Fig. 3.10 (a)). The optical spectrum is centered at 766 nm (Fig. 3.10 (b)). The time-bandwidth product is 2.04 and the corresponding RF spectrum exhibit a 30 dB dynamic contrast (Fig. 3.10 (c)), which indicates a stable mode-locking regime. Under these bias conditions, the average power was 9 mW after collimation, which corresponds to a peak power of 81 mW. As we checked, in the setup at that time, only ~ 80% of the total output of the MLLD was received by the integrating sphere power meter after collimation compared to that directly emitted from the MLLD measured. Taking into account a 20% loss of optical collimation, the peak power of emitted from the MLLD should be about 100 mW in total.

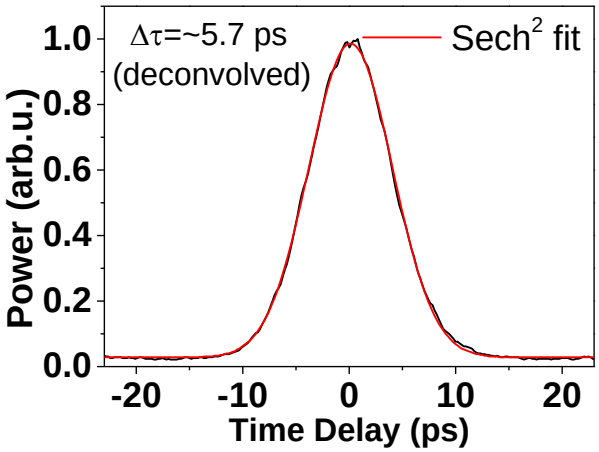

(a)

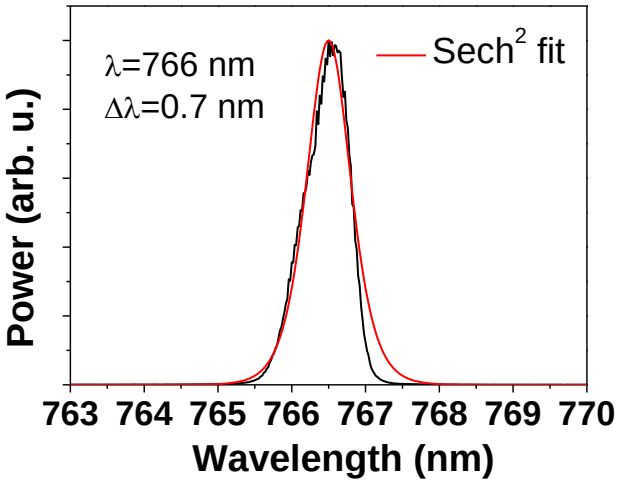

(b)

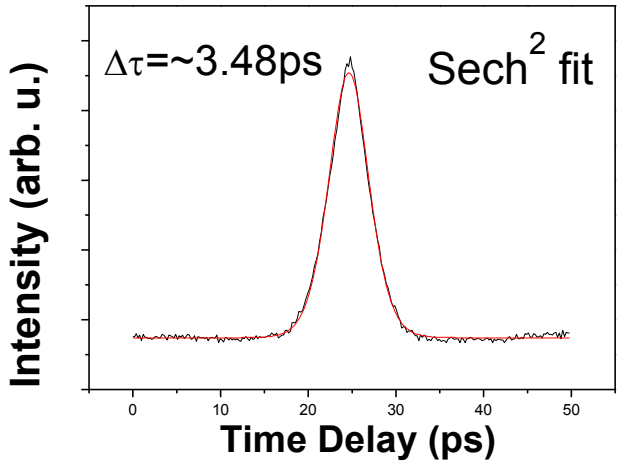

(c)

Fig. 3.10 (a) Autocorrelation trace, (b) optical spectrum and (c) RF spectrum at reverse bias of 2.5 V and forward current of 280 mA.

For a fixed forward bias current of 265 mA, the change of the pulse duration under an increasing reverse bias is shown in Fig. 3.12. The shortest pulse duration of 4.8 ps was achieved under a reverse voltage of 2.6 V and forward current of 265 mA for this device.

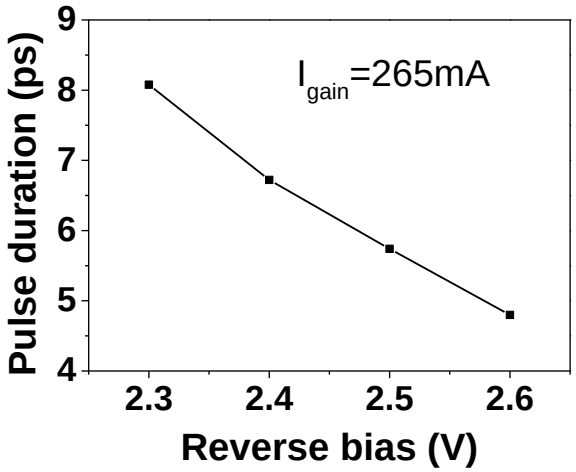

Fig. 3.11 Variation of pulse duration with reverse bias, for a fixed forward current of 265 mA applied to the gain section of the 1815 μm long laser.

The relationship between the current and the gain was also investigated with a fixed reverse bias, as represented in from Fig. 3.13 to Fig. 3.15. With increasing current, the optical spectrum widens. This also leads to shorter pulses until the edge of the stable ML region. From the RF spectra in Fig. 3.14, we can see the RF peaks of stable mode-locking is sharp, narrow and of high intensity, while the peaks of unstable mode-locking is wide, short or have some side peaks. The optical spectra also red-shift as the current is increased, becoming increasingly more asymmetric and developing additional peaks on the red side of the spectra, due to an increase of self-phase modulation with increasing gain [3]. Eventually, at 275 mA the mode-locking regime stability collapses as shown by the autocorrelation, which exhibits a coherence spike on a strong background level which is a signature for continuous noise [4].

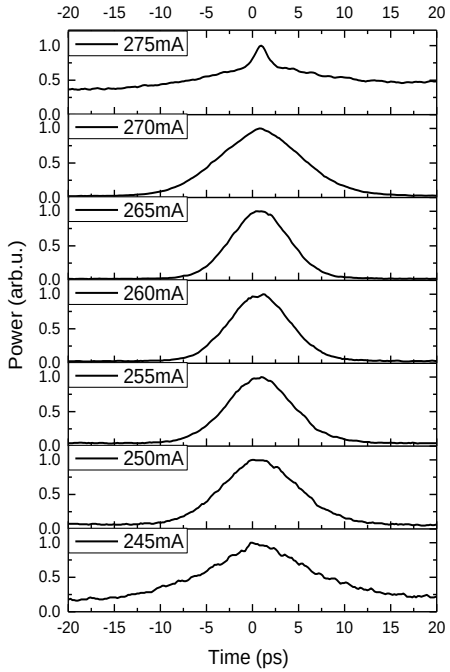

Fig. 3.12 Pulse trace of the 1815 μm long MLLD emitting at 766 nm under a reverse bias of -2.6 V, 10 ℃ and various current levels

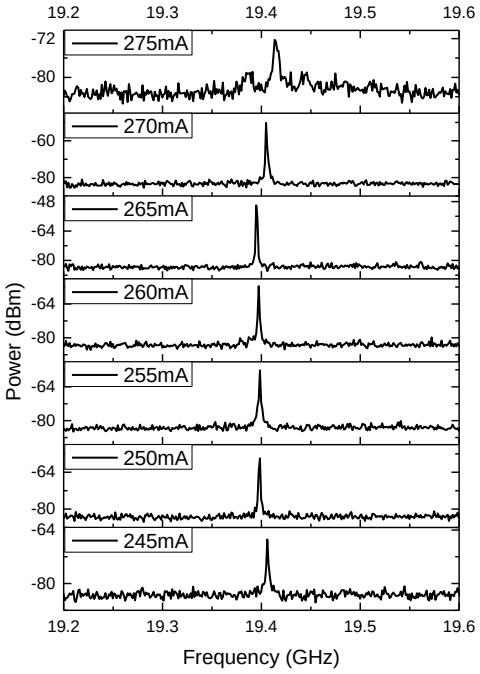

Fig. 3.13 RF spectrum of the 1815 μm long MLLD emitting at 766 nm under a reverse bias of -2.6V, 10 ℃ and various current levels

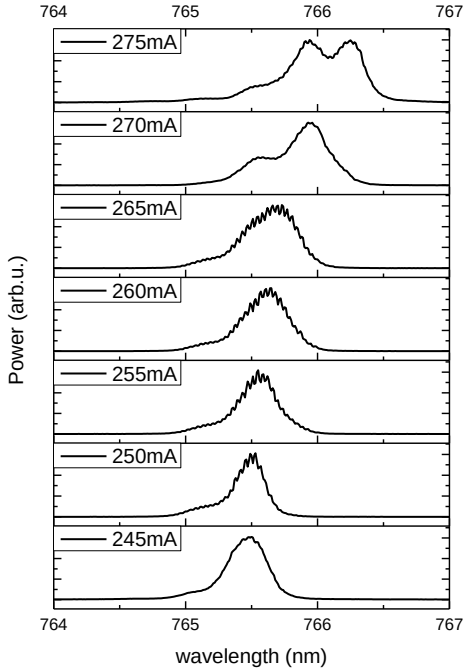

Fig. 3.14 Optical spectrum of the 1815 μm long MLLD emitting at 766 nm under a reverse bias of -2.6V, 10 ℃ and various current levels

We also checked the effect of the reverse bias applied to the saturable absorber with a fixed forward bias current applied to the gain section, as represented in from Fig. 3.16 to Fig. 3.18. With increasing reverse bias, the optical spectrum widens. It is quite obvious that the pulses become narrower when the reverse bias increases. As the RF spectra show in Fig. 3.17, we can also see the peak in the RF spectra of stable mode-locking are sharp, while the peaks of unstable mode-locking are wide, shorter and they have more side peaks. The optical spectra also red-shift as the reverse bias is increased.

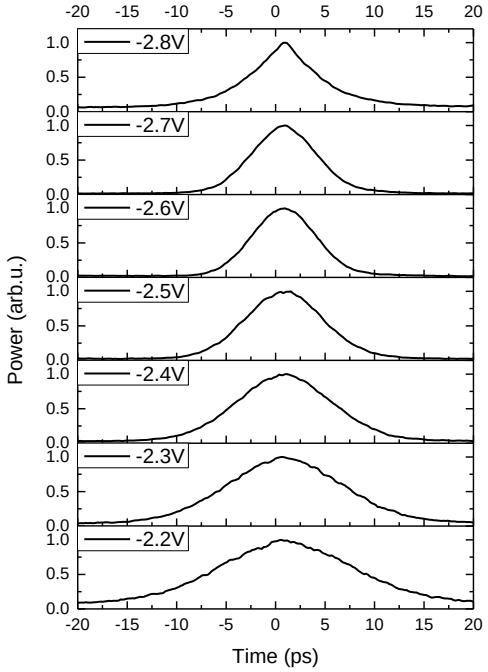

Fig. 3.15 Pulse trace of the 1815 μm long MLLD emitting at 766 nm under 265mA 10 °6 and various reverse bias

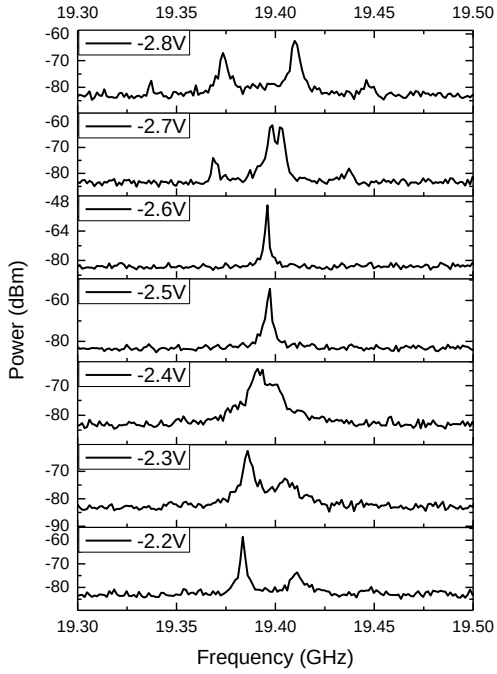

Fig. 3.16 RF spectrum of the 1815 μm long MLLD emitting at 766 nm under 265 mA 10 ℃ and various reverse bias

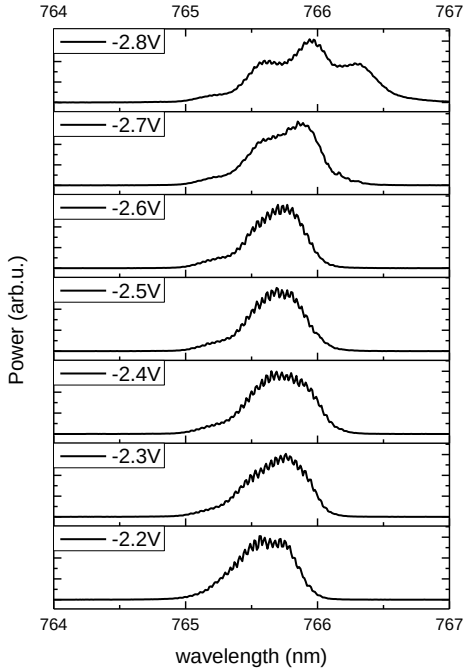

Fig. 3.17 Optical spectrum of the 1815 μm long MLLD emitting at 766 nm under 265mA 10°C and various reverse bias

3.2.2 1515 μm long MLLD emitting at 766 nm

Our 1515 μm long MLLD with exactly the same structure and 15% front facet reflectivity was also mode-locked successfully. Fig. 3.19 (a) shows the light-current characteristics of this chip under 10°C, for various values of reverse bias applied to the saturable absorber section. We detected stable mode-locking when the current ranged from 210 mA to 235 mA, with the reverse bias varying from -2.76 V to -3.04 V. The optical spectra were centered at around 766 nm and the repetition rate was about 23.21 GHz, when the laser is mode-locking stably. The pulse duration is approximately 4 ps. The characteristics of a typical mode-locking regime from the identified stable ML region are shown in Fig. 3.19 (b) to Fig. 3.19 (d). The RF peak is at least 30 dB above the noise floor. We assume $sech^2$ as the pulse shape. The pulse duration was estimated to be 4.17 ps, with the optical spectrum centered at 766.31 nm

and with a bandwidth of 0.65 nm. A time-bandwidth product of 1.39 was achieved. In this case, the average power of 8.3 mW corresponded to a peak power of 75 mW.

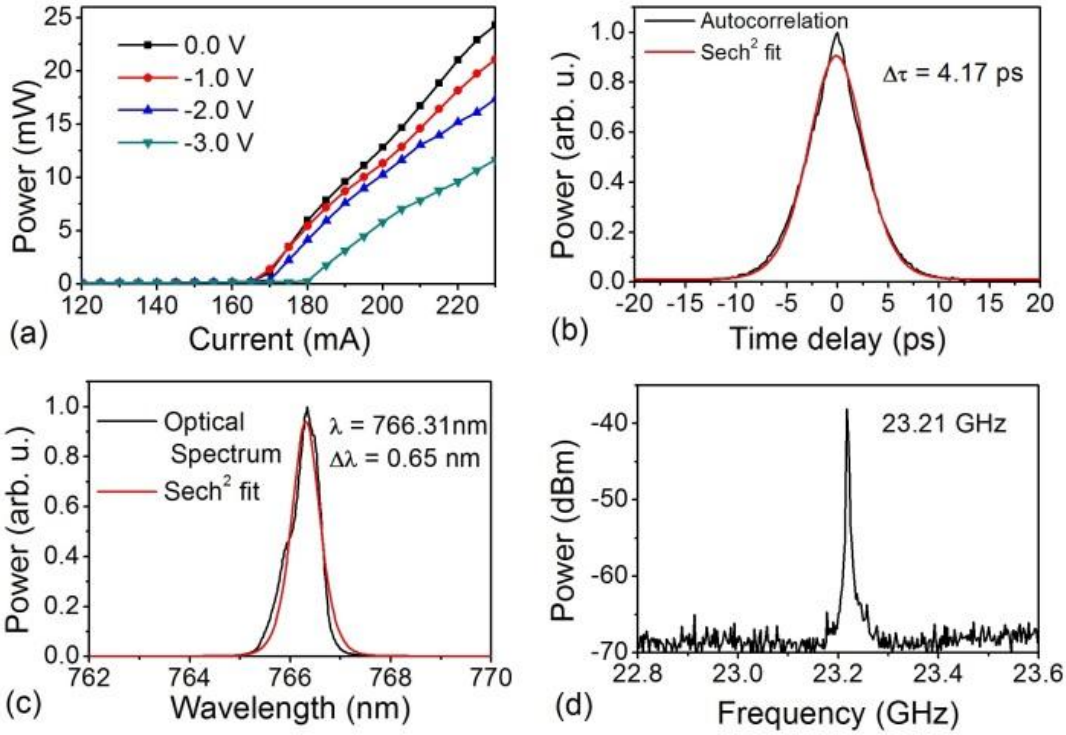

Fig. 3.18 (a) Light-current characteristics of the 1515 um long laser for different reverse bias conditions. (b) Autocorrelation, (c) Optical spectrum and (d) RF spectrum at reverse bias of -3.0 V and forward current of 230 mA.

In a similar fashion to the longer MLLD, the 1515 μm chip tended to generate pulses of a shorter duration with higher reverse bias and lower forward current. However, it was observed that the region of stable mode-locking for the shorter cavity length was quite narrow. It often ranges only a few tens of millivolts of reverse bias under a fixed forward current. This narrower reverse bias region could be due to the stronger constraints imposed on the absorption/gain processes by the higher pulse repetition rate. On one hand, to satisfy the background stability criterion, the reverse bias should be high enough in order to speed up the absorption recovery time, which should be shorter than both the gain recovery time and the pulse cavity round trip time,

which is about 43 ps. On the other hand, the increase in reverse bias leads to a shift in absorption, induced by quantum confined Stark effect (QCSE), and the increase in absorption saturation energy. So, this imposes an upper limit to the reverse bias which enables a stable ML regime.

3.3 Brief summary of the results

We have demonstrated the first mode-locked semiconductor laser diode emitting in the spectral wavelength range of 760 nm. Emission wavelength at 766 nm and stable 19.4 GHz pulse train with pulse duration of about 5 picoseconds were obtained when the cavity length was 1.8 mm. Pulse train with emission wavelength at 766 nm, a stable 23 GHz repetition rate and pulse duration of 4.17 picoseconds were obtained when the cavity length was 1.5 mm.

3.4 References

[1] Kyoung Chan Kim. et al., "Performance improvement of high-power AlGaAs laser," *Journal of the Korean Physical Society*. Vol. 47, pp. S572-S575, 2005.

[2] Tianhong Xu, Paolo Bardella, and Ivo Montrosset, "Quantum Dot Passively Mode-Locked Laser Optimization for High-Power and Short Pulses," *IEEE Photonics Technology Letters*, vol. 25, no. 1, January 1, 2013

[3] G. P. Agrawal and N. A. Olsson, "Self-phase modulation and spectral broadening of optical pulses in semiconductor-laser amplifiers," *IEEE J. Quantum Electron.* **25** (11), 2297–2306, 1989.

[4] E. P. Ippen and C. V. Shank, "Techniques for measurement," in *Ultrashort Light Pulses*, S. L. Shapiro, ed. Springer Berlin, pp. 83–122, 1984.

4. 750-nm Mode-Locked Laser Diodes

4.1 Device structure and fabrication

In order to access the 750-nm spectral band, the composition of the quantum wells was changed to $Al_{0.12}Ga_{0.88}As$, while the barriers were kept at $Al_{0.3}Ga_{0.7}As$, in order to achieve a shorter wavelength. The material structure for the wafer reference CCS-1093 is shown by Fig. 4.1, below.

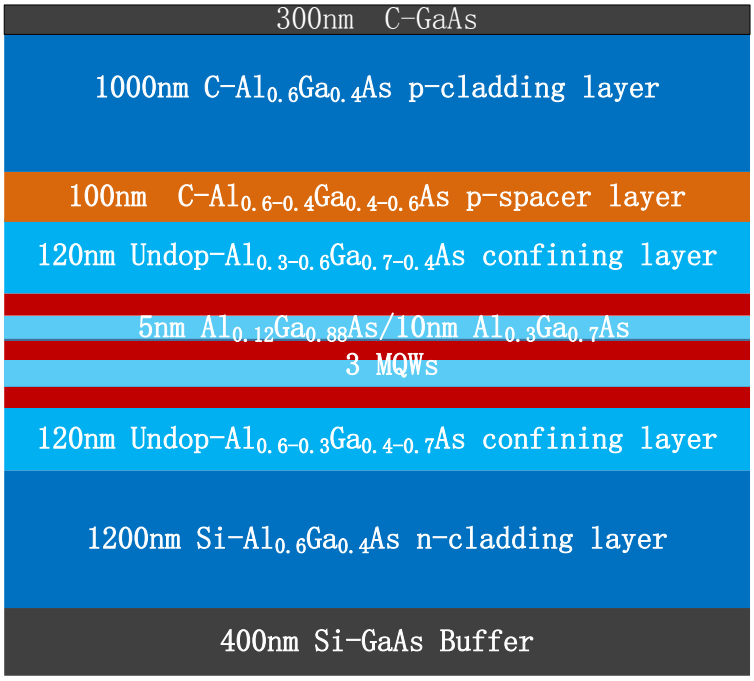

Fig. 4.1 Material structure of CCS-1093

4.2 Experimental results

Four groups of 750-nm MLLD chips were fabricated in total, with two different reflectivities and two different cavity lengths, as shown in Table 4.1. The chips identified in red have been tested by us. The tests showed that, similarly to the 760-nm MLLDs, the chips with 6.6% reflectivity did not display mode-locked

operation.

Table 4.1 List of all the 750-nm MLLD chips

	AR 6.6%			AR 15%		
CCS-1093 1.8mm	1-1	1-2	1-3	**1-1**	**1-2**	1-3
CCS-1093 1.5mm	4-1	4-2	4-3	**4-1**	4-2	4-3

4.2.1 1815 μm long MLLD emitting at 752 nm

Slightly shorter pulse lengths were generated from the 752-nm MLLD on the material structure as compared with the similar device structure (1.8 mm cavity length) fabricated from the 766 nm-material structure. However, the output average power and peak power from the MLLD based on the 752-nm material structure was somewhat lower, which can possibly be attributed to lower material gain and higher internal loss in 752-nm material structure.

The light-current characteristics of this laser are shown in Fig. 4.2 (a). At 10 ^{o}C, a stable mode-locking regime for different currents from 250 mA to 300 mA is reached and under values of reverse bias between 2.7 V and 3.05 V (depending on the forward current), in agreement with the observed strong absorption in Fig. 4.2 (a). Typical features of the pulsed output in the stable mode-locking region are observed, shown in Fig. 4.2 (b) - (d). The pulse duration of 3.5 ps was achieved under a reverse bias of 2.83 V and forward current of 260 mA, as shown in Fig. 4.2 (b), while the optical spectrum is centered at 752 nm (Fig. 4.2 (c)), with an optical bandwidth of 0.62 nm, this results in a time-bandwidth product of 1.30. The pulse repetition frequency was 19.4 GHz, as shown in the frequency range in Fig. 4.2 (d). For this bias condition, the average power after collimation was 4.7 mW, corresponding to a peak power of 68.5 mW. Taking into account of the 20% loss from the optical collimation,

the achievable peak power of the chip should be a little more than 85 mW. The shortest pulse duration for this device was measured at 3.3 ps, which was obtained under a reverse bias of 3.04 V and forward current of 250 mA. However, the average power was only 3.37 mW resulting in a peak power of 52.6 mW and the mode-locking was not fully stable.

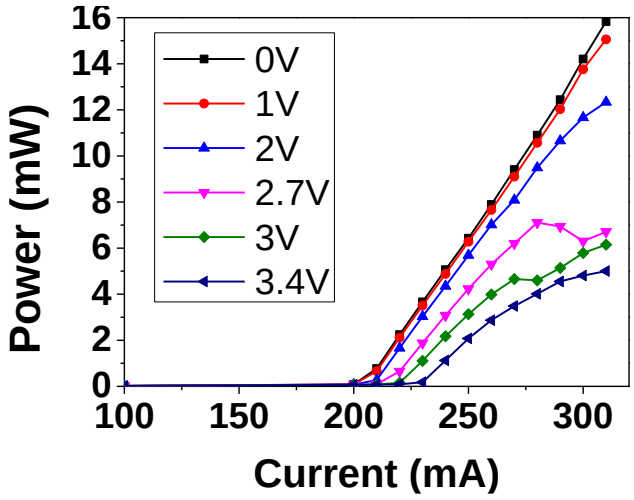

(a)

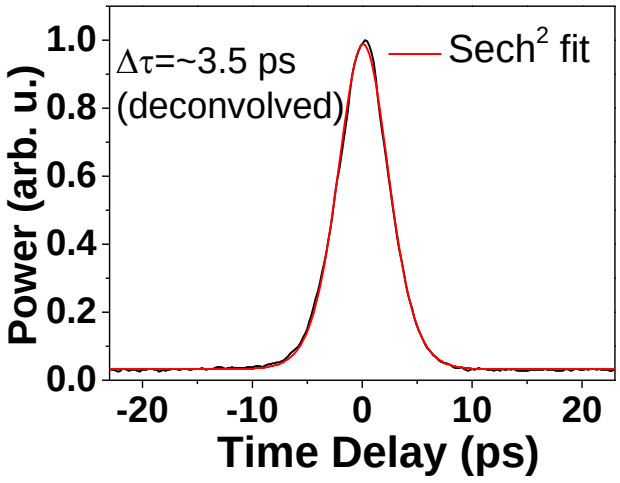

(b)

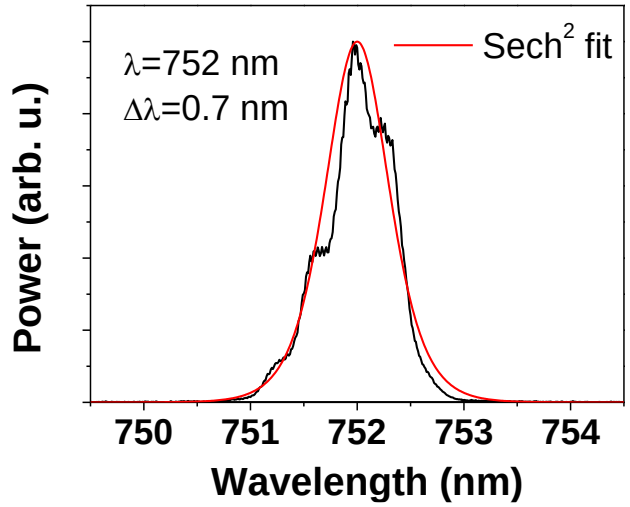

(c)

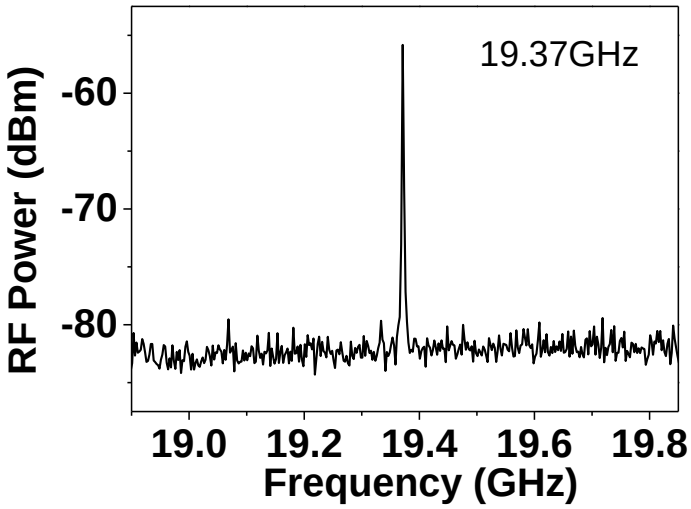

(d)

Fig. 4.2 (a) Light-current characteristics of the 1815μm long for different reverse-bias conditions at 752 nm. (b) Autocorrelation trace at reverse bias of 2.83 V and forward current of 260 mA. (c) Corresponding optical spectrum. (d) Corresponding RF spectrum.

We checked the effect of the reverse bias applied to the saturable absorber of this chip. Fig. 4.3 shows the pulse durations while a fixed gain current of 280 mA and various reverse bias values were applied to the saturable absorber.

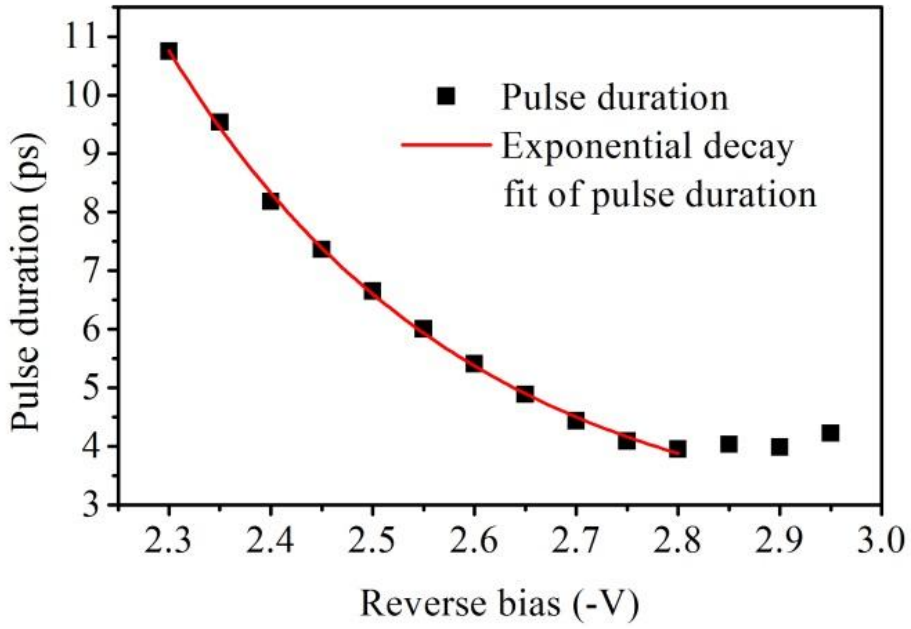

Fig. 4.3 Variation in pulse duration with reverse bias applied to the saturable absorber, for a fixed gain current of 280 mA.

It is observed that the pulse duration decreased with an increasing reverse bias, with an exponential trend. This behavior can be explained by the fact that the absorption recovery time also decreases exponentially with reverse bias [1] and the pulse duration has a linear relationship with the absorption recovery time [2, 3]. Beyond -2.8V, the pulse duration does not reduce more, even though the absorption recovery may continue to decrease. This was predicted theoretically before [4, 5] and could be related with weaker absorption saturation in these conditions.

In addition, we checked the pulse repetition rate under various reverse bias and a fixed forward current, various currents and a fixed reverse bias respectively, shown, in Fig. 4.4.

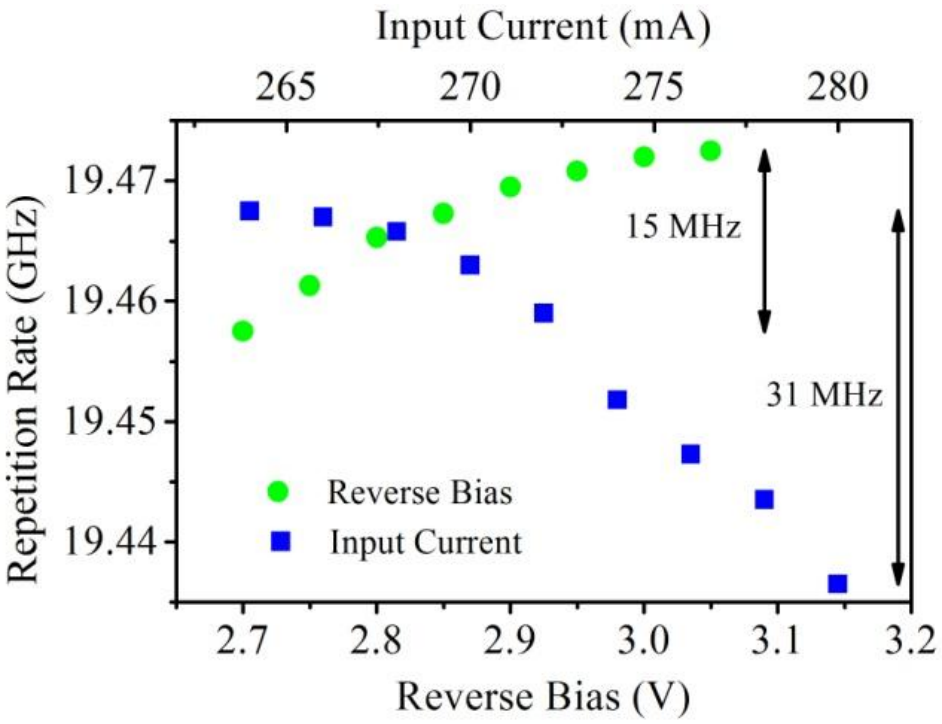

Fig. 4.4 Tunability of the pulse repetition rate with change of reverse bias (under fixed gain current of 268 mA) and input current (under fixed reverse bias of 2.80 V).

When the forward current is fixed at 268 mA, the repetition rate increased with reverse bias that applied to the saturable absorber, and it decreased with increasing current applied to the gain section. These effects can be explained by the interplay between gain and absorption saturation effects and the pulse energy, which lead to a temporal shift of the pulse envelope [6]. This feature can be used to tune the pulse repetition rate from the chips. The tuning range is 15 MHz while the current is fixed and 31 MHz while the reverse bias is fixed. The repetition rate of the semiconductor laser is determined mainly by the length of the cavity. The cavity length cannot be that accurate after cleaving. So this allows us to tune the repetition rate to the frequency that is necessary for the application (this can be particularly important for optical communications).

4.2.2 1515 μm long MLLD emitting at 752 nm

The chip of the same structure but with 1515 μm long cavity length was also mode-locked successfully. Fig. 4.5 shows the light-current characteristics of this chip under 10 ℃, for various values of reverse bias applied to the saturable absorber section. Obvious optical absorption in the performance was observed when the reverse bias is over 2 V.

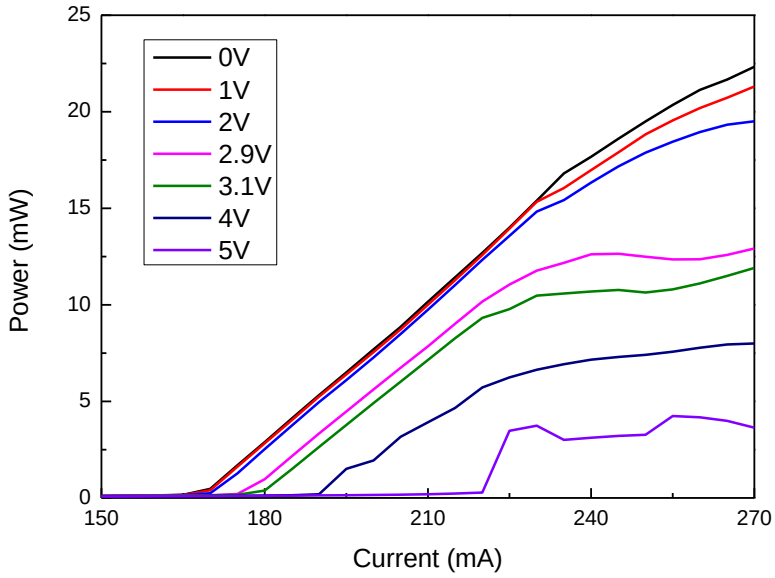

Fig. 4.5 P-I curves of the 1515 μm long MLLD emitting at 752 nm under 10 °l and various reverse bias

The optical spectra of this chip are centered at around 752 nm too, with a repetition rate of about 23.11 GHz, when the laser is mode-locking stably. The pulse duration is approximately 3.4 to 3.6 ps. The characteristics of two typical mode-locking regimes from the identified stable ML region are shown in Fig. 4.6 and Fig 4.7. In Fig 4.6, 215 mA forward current and 3 V reverse bias were applied to the chip. The average power was 9.93 mW. The RF peak was at 23.11 GHz which was at least 30 dB above the noise floor. We assume $sech^2$ as the pulse shape. The pulse

duration was estimated to be 3.6 ps, with the optical spectrum centered at 751.64 nm.

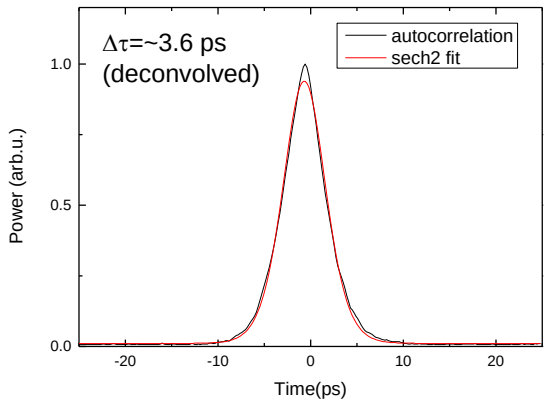

(a)

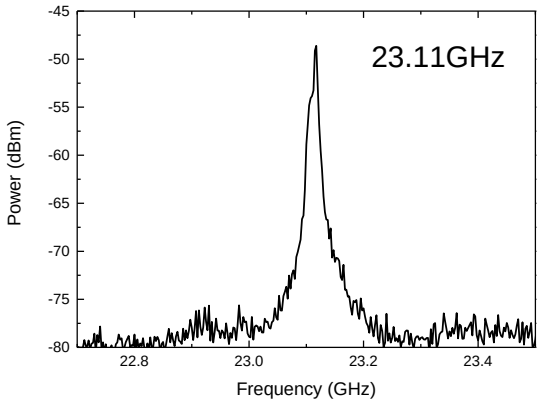

(b)

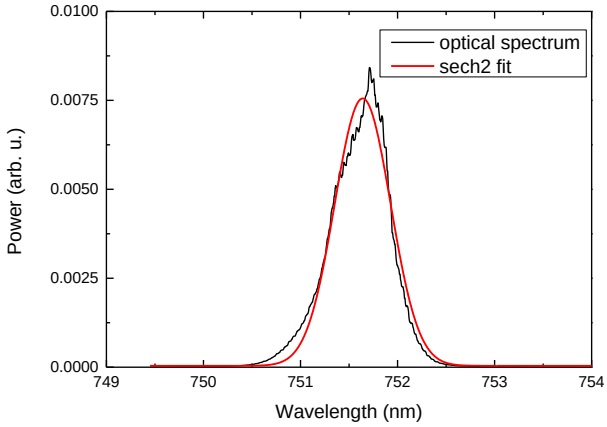

(c)

Fig. 4.6 (a) Autocorrelation trace at 10 ℃, reverse bias of 3 V and forward current of 215 mA. (b) Corresponding RF spectrum. (c) Corresponding optical spectrum.

In Fig 4.7, 215 mA forward current and 3.8 V reverse bias were applied to the chip. The average power was 10.25 mW, leading to a peak power of 130.5 mW The RF peak was at 23.10 GHz which was approximately 35 dB above the noise floor. We assume $sech^2$ as the pulse shape. The pulse duration was estimated to be 3.4 ps, with the optical spectrum centered at 751.44 nm. The optical spectral bandwidth is 0.33 nm.

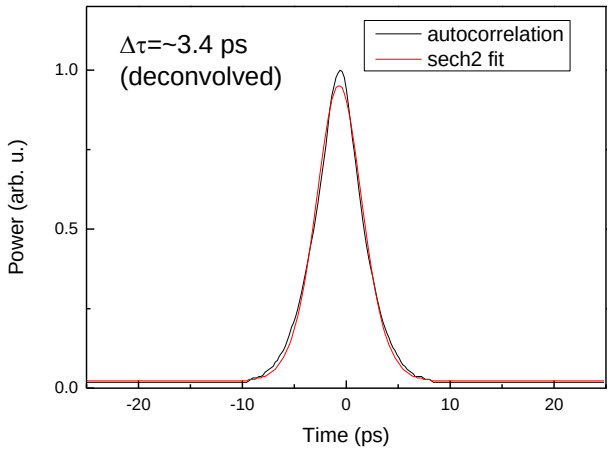

(a)

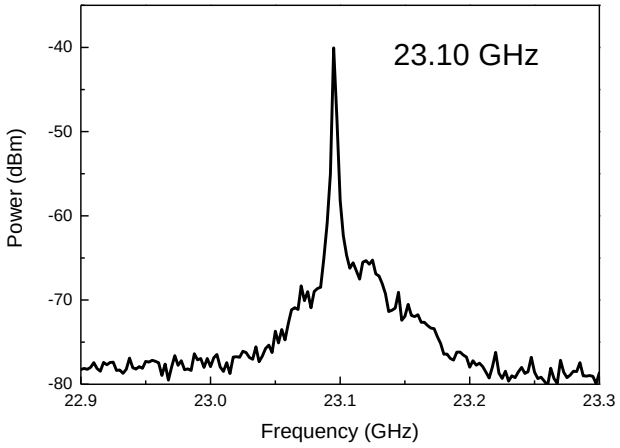

(b)

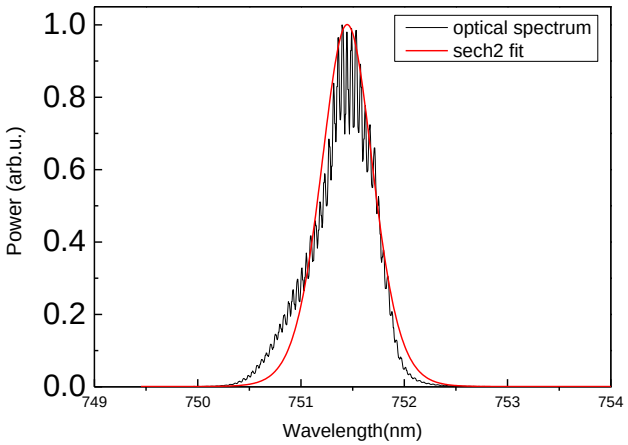

(c)

Fig. 4.7 (a) Autocorrelation trace at 10 ℃, reverse bias of 2.8 V and forward current of 215 mA. (b) Corresponding RF spectrum. (c) Corresponding optical spectrum.

Further results are also presented in Appendix.

4.3 Brief summary of the results

We have demonstrated the first mode-locking semiconductor laser diode emitting in the spectral wavelength range of 750 nm. Emission wavelength at 752 nm and stable 19.4 GHz pulse train with a pulse duration of down to 3.5 picoseconds were obtained when the cavity length was 1.8 mm. Emission wavelength at 752 nm and a stable 23 GHz pulse train with a pulse duration of 3.4 picoseconds were obtained when the cavity length was 1.5 mm.

4.4 References

[1] J. R. Karin, R. J. Helkey, D. J. Derickson, R. Nagarajan, D. S. Allin, J. E. Bowers, and R. L. Thornton, *Appl. Phys. Lett*. 64(6), 676–678, 1994.

[2] K. A. Williams, M. G. Thompson, and I. H. White, *New J. Phys*. 6, 179, 2004.

[3] M. A. Cataluna, D. B. Malins, A. Gomez-Iglesias et al., “Temperature

dependence of electroabsorption dynamics in an InAs quantum-dot saturable absorber at 1.3 μm and its impact on mode-locked quantum-dot lasers," *Applied Physics Letters*, vol. 97, no. 12, pp. 121110, 2010.

[4] W. Yang, and A. Gopinath, "Study of passive mode locking of semiconductor lasers using time‐domain modeling," *Applied Physics Letters*, vol. 63, no. 20, pp. 2717-2719, 1993.

[5] D. J. Jones, L. M. Zhang, J. E. Carroll et al., "Dynamics of monolithic passively mode-locked semiconductor lasers," *Quantum Electronics, IEEE Journal of*, vol. 31, no. 6, pp. 1051-1058, 1995.

[6] S. Arahira, and Y. Ogawa, "Repetition-frequency tuning of monolithic passively mode-locked semiconductor lasers with integrated extended cavities," *Quantum Electronics, IEEE Journal of*, vol. 33, no. 2, pp. 255-264, 1997.

5. Summary and outlook

5.1 Summary

In this work, four types of semiconductor mode-locking laser diodes have been investigated. The main characteristics of these four types of lasers are shown in table 5.1.

Table 5.1 Summary of the mode-locking performance

Chips wavelength/ length	Pulse duration (ps)	Center wavelength (nm)	Spectral bandwidth (nm)	Average power (mW)	Peak power (mW)
766-nm 1815μm	5.7	766	0.7	11.3	90
766-nm 1515μm	4.17	766.31	0.65	8.3	75
752-nm 1815μm	3.5	752	0.62	5.9	85
752-nm 1515μm	3.4	751.44	0.33	10.25	130.5

With the 766-nm chips, we have demonstrated the first mode-locked semiconductor lasers operating at the spectral waveband of 760 nm. Two different cavity lengths of 1815 μm and 1515 μm were tested and both enabled the generation of ultrashort pulses with a central wavelength at 766 nm, with pulse durations down to approximately 4 ps.

With the 752-nm chips, we have demonstrated the first deep-red semiconductor monolithic mode-locked lasers. Also two different cavity lengths of 1815μm and 1515 μm were tested and both enabled the generation of ultrashort pulses with a central wavelength at 752 nm, with pulse durations down to approximately 3.4 ps. Even more, this represents also the shortest wavelength generated directly by an ultrafast edge-emitting laser in the red to near-infrared spectral region.

The mode-locking characteristics were investigated as a function of the bias, which can be explained by the interplay of dynamic gain and loss processes. The role of the front facet reflectivity was also found to be instrumental in ensuring a stable mode-locking regime without self-pulsations. This spectral waveband is of relevance for pulsed THz generation, optical communications and multi-photon imaging of skin and muscular tissue. And as such, this demonstration paves the way for the future development of an all-semiconductor master-oscillator power amplifier, which would allow the use of such a compact laser system in a clinical setting.

5.2 Future investigations

Although we have demonstrated several types of semiconductor mode-locking lasers, their performance still has space to be improved, especially compared to solid-state mode-locking lasers. One possibility for future work would be to investigate the performance of similar laser diodes with different reflectivities in the front facet, as it was noted that this was important to achieve mode-locking. On one hand, higher reflectivity leads to lower output power, but on the other hand the higher intracavity power could potentially lead to stronger saturation of the absorber and shorter pulse durations, as predicted theoretically. It would be interesting to understand the trade-off between these two factors to optimize the output peak power.

During the process of all my experiments, I also found the performances of the lasers is quite sensitive to temperature. So, improving the packaging to improve the heat dissipation could also potentially improve the characteristics of the MLLDs.

Appendix

We checked how the autocorrelation trace, RF spectrum and optical spectrum changed when the reverse bias applied to the saturable absorber changed, with a fixed forward bias current applied to the gain section, for the 750-nm MLLD with 1515 μm cavity length, 15% AR, under 10 ℃. The forward current was fixed at 210 mA and 220 mA respectively, as represented in Fig. 6.1 to Fig. 6.6.

We also checked how those characteristics changed when the forward current changed with a fixed reverse bias on the same chip under 10 °C. The reverse bias was fixed at 2.9 V and 3.1 V respectively, as represented in Fig. 6.7 to Fig. 6.12.

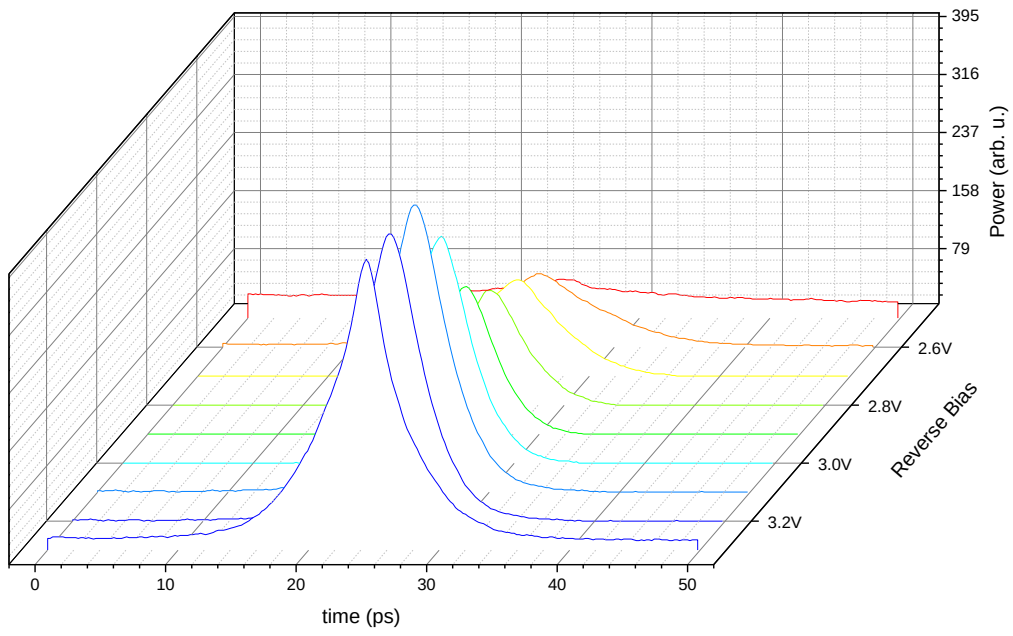

Fig. 6.1 Autocorrelation traces of the 1515 μm long MLLD emitting at 752 nm under 210 mA, 10 ℃ and various reverse bias.

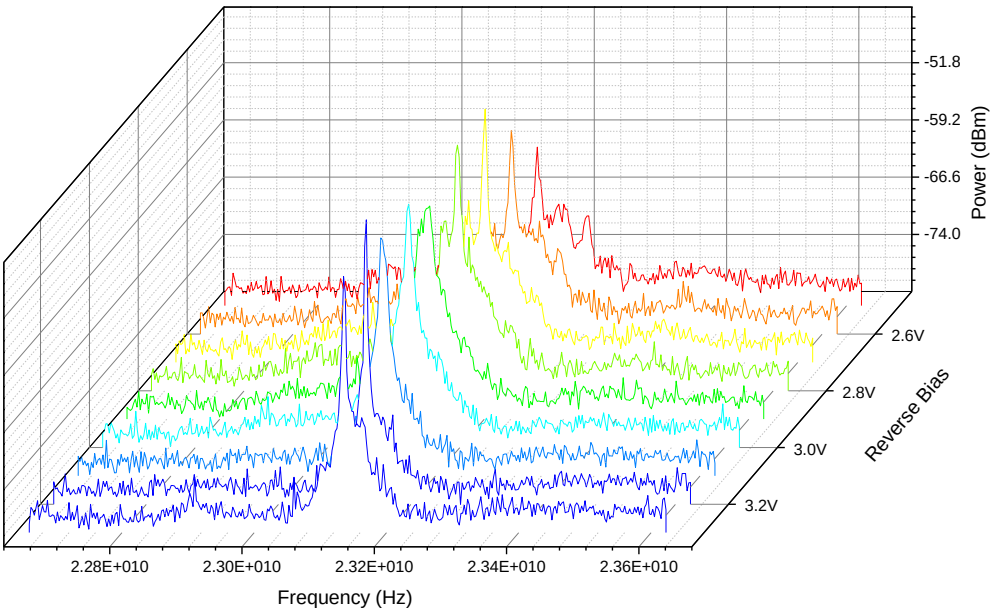

Fig. 6.2 RF spectra of the 1515 μm long MLLD emitting at 752 nm under 210 mA, 10 ℃ and various reverse bias.

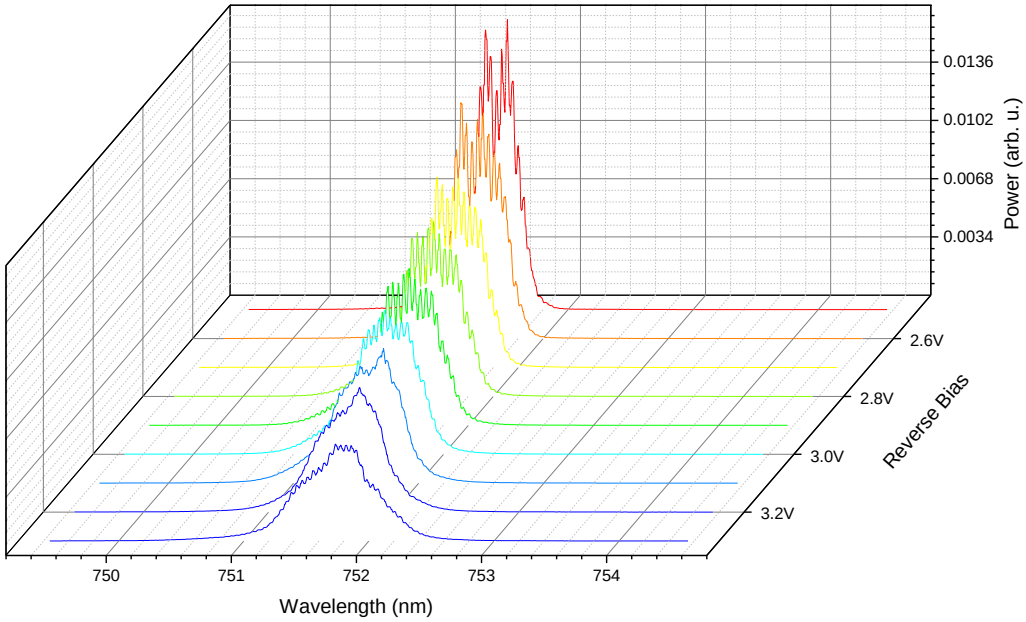

Fig. 6.3 Optical spectra of the 1515 μm long MLLD emitting at 752 nm under 210 mA, 10 ℃ and various reverse bias.

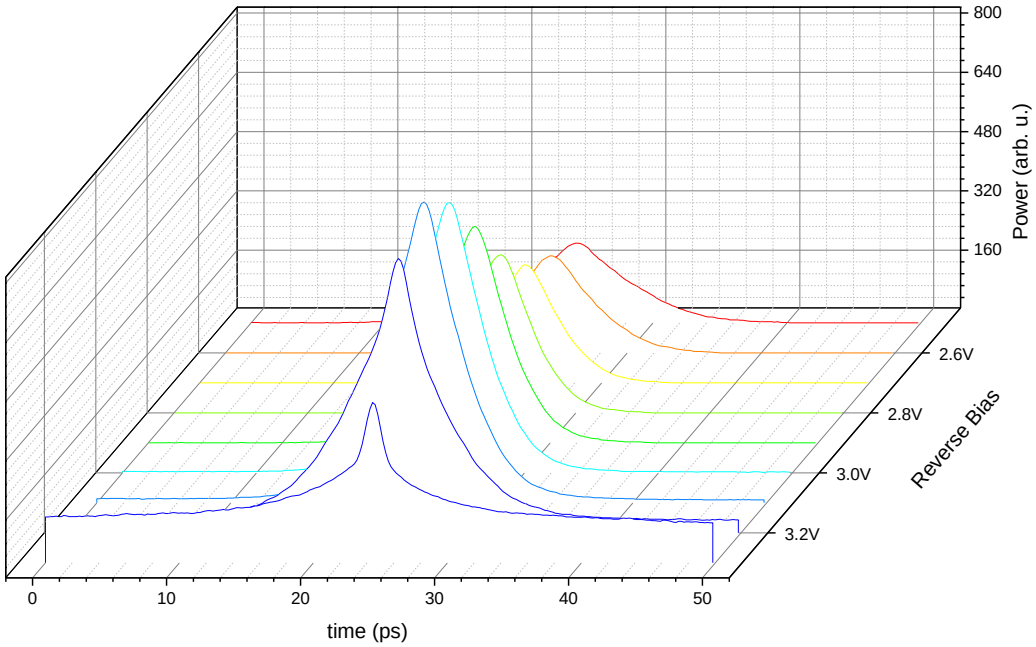

Fig. 6.4 Autocorrelation traces of the 1515 μm long MLLD emitting at 752 nm under 220 mA, 10 ℃ and various reverse bias.

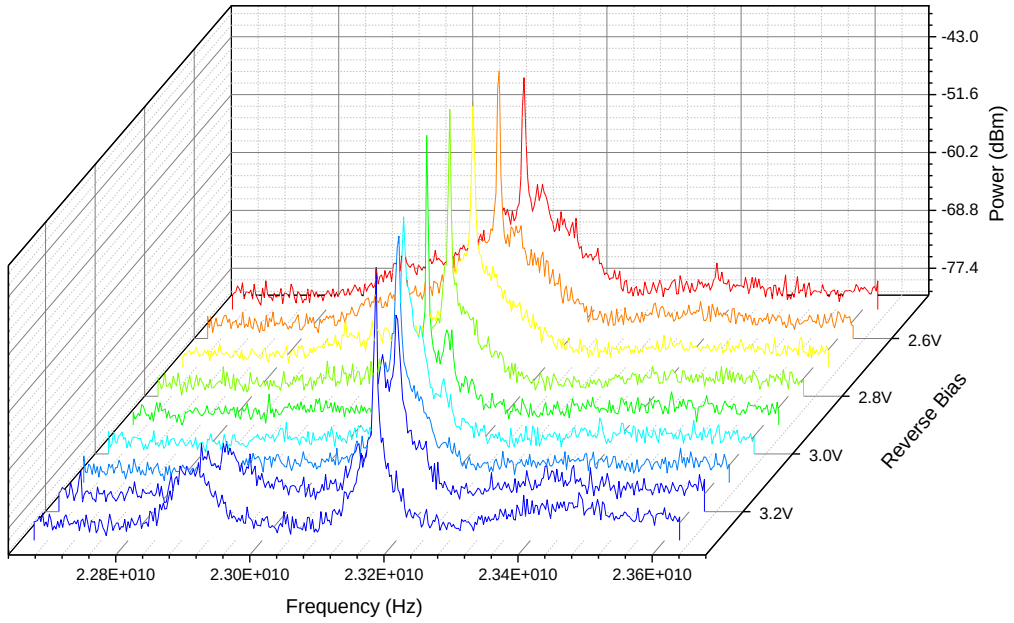

Fig. 6.5 RF spectra of the 1515 μm long MLLD emitting at 752 nm under 220 mA, 10 ℃ and various reverse bias.

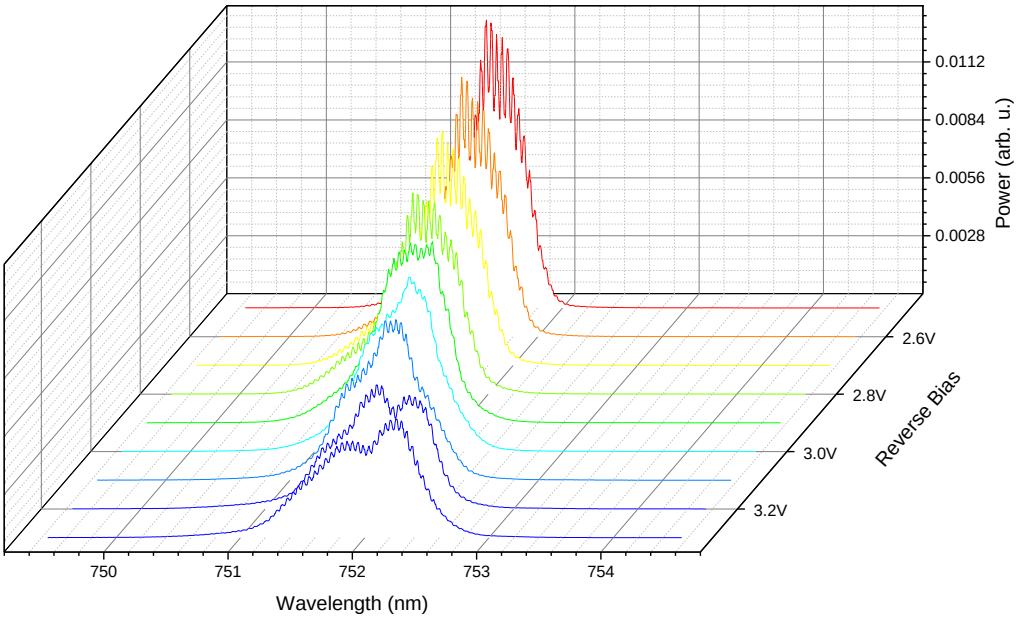

Fig. 6.6 Optical spectra of the 1515 μm long MLLD emitting at 752 nm under 220mA, 10 ℃ and various reverse bias.

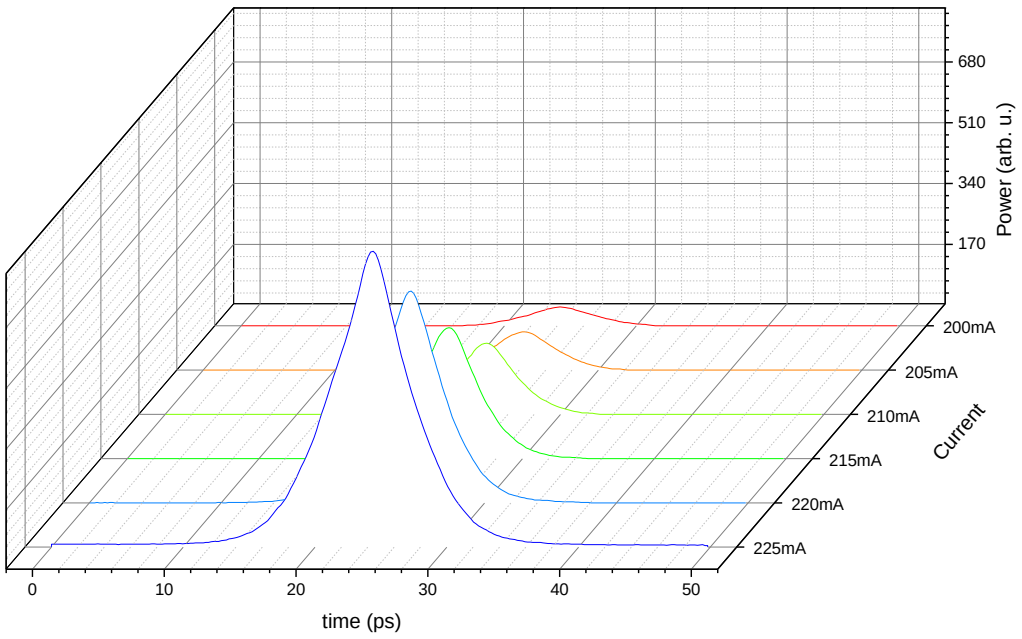

Fig. 6.7 Autocorrelation traces of the 1515 μm long MLLD emitting at 752 nm under -2.9 V, 10 ℃ and various current values.

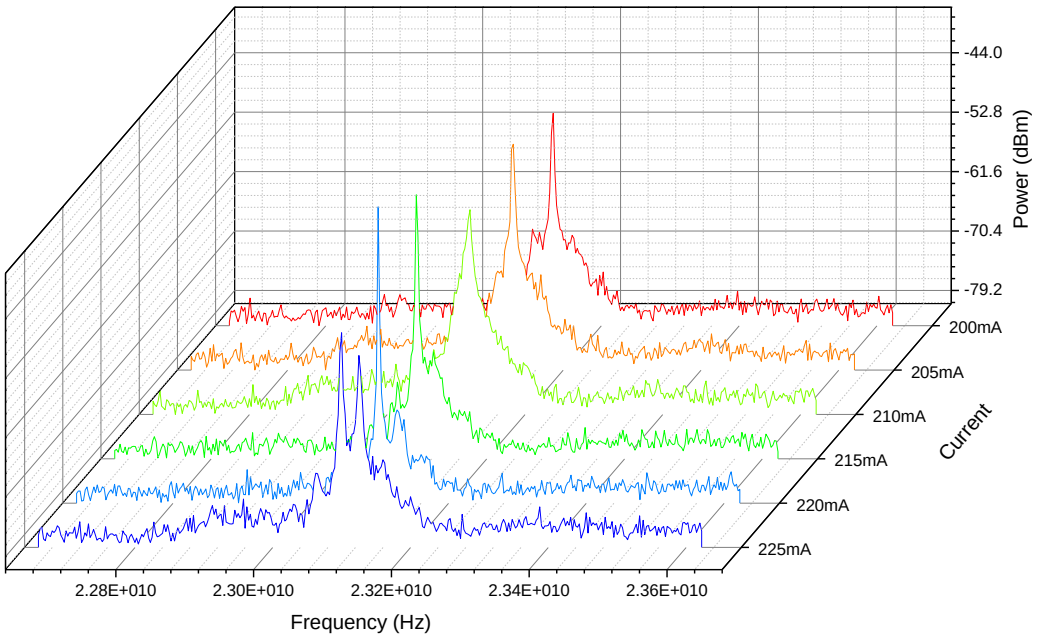

Fig. 6.8 RF spectra of the 1515 μm long MLLD emitting at 752 nm under -2.9 V, 10 ℃ and various current values.

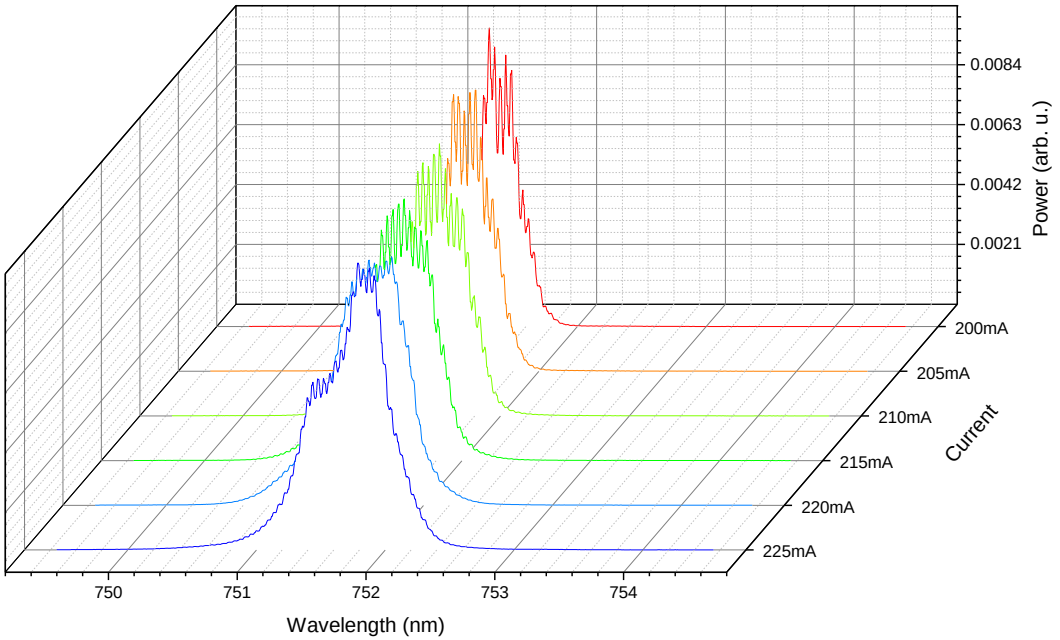

Fig. 6.9 Optical spectra of the 1515 μm long MLLD emitting at 752 nm under -2.9 V, 10 ℃ and various current values.

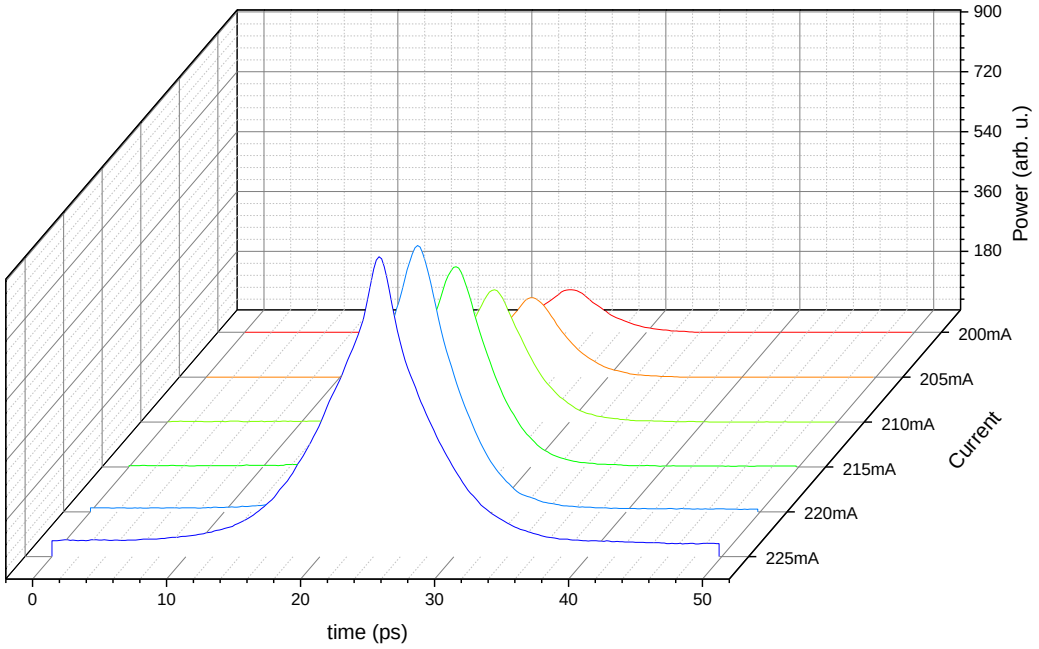

Fig. 6.10 Autocorrelation traces of the 1515 μm long MLLD emitting at 752 nm under -3.1 V, 10 ℃ and various current values.

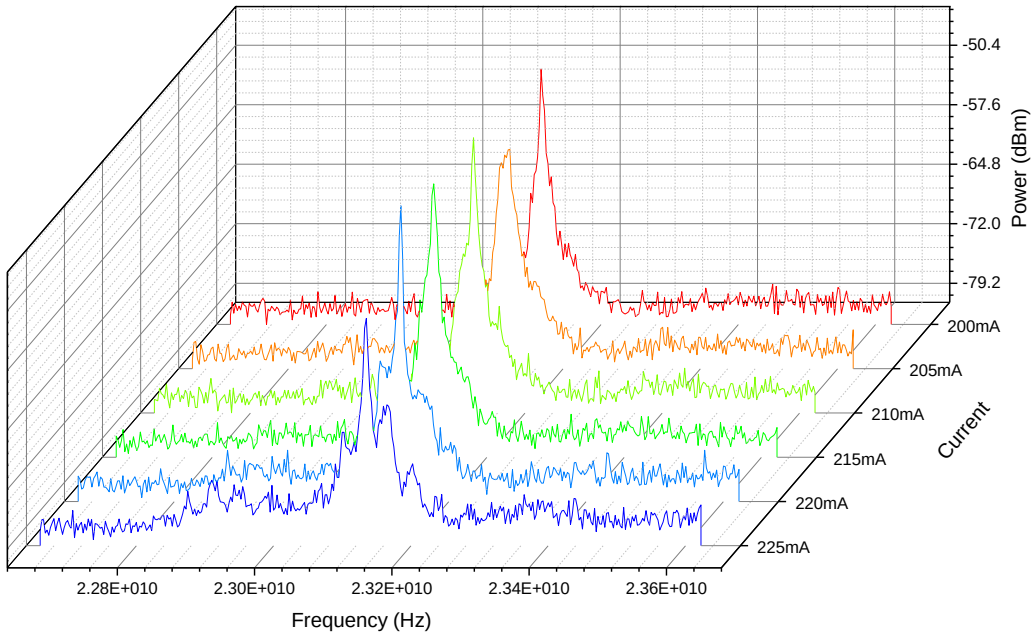

Fig. 6.11 RF spectra of the 1515 μm long MLLD emitting at 752 nm under -3.1 V, 10 ℃ and various current values.

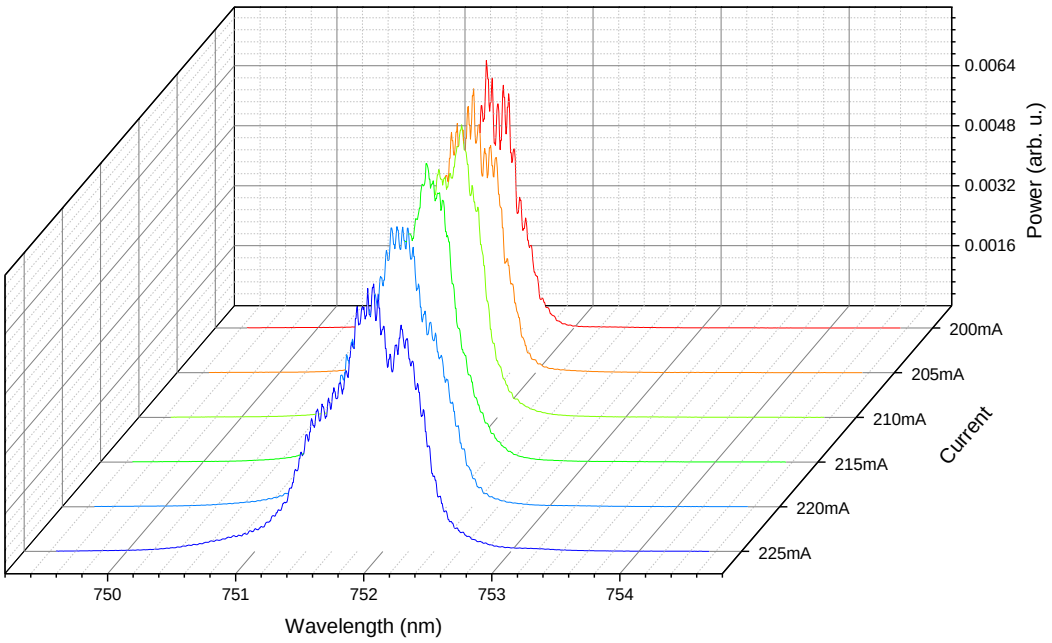

Fig. 6.12 Optical spectra of the 1515 μm long MLLD emitting at 752 nm under -3.1 V, 10 ℃ and various current values.